



LJMU Research Online

Davies, B, Kudritzki, R-P, Plez, B, Trager, S, Lancon, A, Gazak, Z, Bergemann, M, Evans, C and Chiavassa, A

The Temperatures Of Red Supergiants

<http://researchonline.ljmu.ac.uk/id/eprint/1644/>

Article

Citation (please note it is advisable to refer to the publisher's version if you intend to cite from this work)

Davies, B, Kudritzki, R-P, Plez, B, Trager, S, Lancon, A, Gazak, Z, Bergemann, M, Evans, C and Chiavassa, A (2013) The Temperatures Of Red Supergiants. *Astrophysical Journal*, 767 (3). ISSN 0004-637X

LJMU has developed **LJMU Research Online** for users to access the research output of the University more effectively. Copyright © and Moral Rights for the papers on this site are retained by the individual authors and/or other copyright owners. Users may download and/or print one copy of any article(s) in LJMU Research Online to facilitate their private study or for non-commercial research. You may not engage in further distribution of the material or use it for any profit-making activities or any commercial gain.

The version presented here may differ from the published version or from the version of the record. Please see the repository URL above for details on accessing the published version and note that access may require a subscription.

For more information please contact researchonline@ljmu.ac.uk

<http://researchonline.ljmu.ac.uk/>

THE TEMPERATURES OF RED SUPERGIANTS

BEN DAVIES^{1,2,3}, ROLF-PETER KUDRITZKI⁴, BERTRAND PLEZ⁵, SCOTT TRAGER⁶, ARIANE LANÇON⁷,
ZACH GAZAK⁴, MARIA BERGEMANN⁸, CHRIS EVANS⁹, ANDREA CHIAVASSA¹⁰

¹Astrophysics Research Institute, Liverpool John Moores University, Egerton Wharf, Birkenhead, CH41 1LD, UK.

²Institute of Astronomy, University of Cambridge, Madingley Road, Cambridge CB3 0HA, UK.

³School of Physics & Astronomy, University of Leeds, Woodhouse Lane, Leeds LS2 9JT, UK.

⁴Institute for Astronomy, University of Hawaii, 2680 Woodlawn Drive, Honolulu, HI, 96822, USA

⁵Laboratoire Univers et Particules de Montpellier, Université Montpellier 2, CNRS, F-34095 Montpellier, France

⁶Kapteyn Institute, University of Groningen, P.O. Box 800, 9700 AV Groningen, The Netherlands

⁷Observatoire astronomique and CNRS UMR 7550, Université de Strasbourg, Strasbourg, France

⁸Max-Planck-Institute for Astrophysics, Karl-Schwarzschild-Str.1, D-85741 Garching, Germany

⁹UK Astronomy Technology Centre, Royal Observatory Edinburgh, Blackford Hill, Edinburgh., EH9 3HJ, UK; Institute for Astronomy, Royal Observatory Edinburgh, Blackford Hill, Edinburgh., EH9 3HJ, UK and

¹⁰Université de Nice Sophia-Antipolis, Observatoire de la Côte d'Azur, CNRS Laboratoire Lagrange, BP 4229, 06304, Nice Cedex 4, France

Draft version February 13, 2013

ABSTRACT

We present a re-appraisal of the temperatures of Red Supergiants (RSGs) using their optical and near-infrared spectral energy distributions (SEDs). We have obtained data of a sample of RSGs in the Magellanic Clouds using VLT+XSHOOTER, and we fit MARCS model atmospheres to different regions of the spectra, deriving effective temperatures for each star from (a) the TiO bands, (b) line-free continuum regions of the spectral energy distributions (SEDs), and (c) the integrated fluxes. We show that the temperatures derived from fits to the TiO bands are systematically *lower* than the other two methods by several hundred Kelvin. The TiO fits also dramatically over-predict the flux in the near-IR, and imply extinctions which are anomalously low compared to neighbouring stars. In contrast, the SED temperatures provide good fits to the fluxes at all wavelengths other than the TiO bands, are in agreement with the temperatures from the flux integration method, and imply extinctions consistent with nearby stars. After considering a number of ways to reconcile this discrepancy, we conclude that 3-D effects (i.e. granulation) are the most likely cause, as they affect the temperature structure in the upper layers where the TiO lines form. The continuum, however, which forms at much deeper layers, is apparently more robust to such effects. We therefore conclude that RSG temperatures are much warmer than previously thought. We discuss the implications of this result for stellar evolution and supernova progenitors, and provide relations to determine the bolometric luminosities of RSGs from single-band photometry.

Subject headings: Stars: fundamental parameters, Stars: atmospheres, Stars: late-type, Stars: massive, supergiants, Stars: evolution

1. INTRODUCTION

Red Supergiants (RSGs) are a post main-sequence (MS) phase of stars with masses $\sim 8\text{--}30M_{\odot}$ (e.g. Meynet & Maeder 2000; Eldridge et al. 2008; Brott et al. 2011). Their luminosities ($\gtrsim 10^{4.5\text{--}5.8}L_{\odot}$ Humphreys & Davidson 1979) rival those of globular clusters and dwarf galaxies, and dominate the light output of their host galaxies at near-infrared (IR) wavelengths. For most stars in this mass range, the RSG phase is thought to be the evolutionary stage immediately preceding core-collapse supernova (SN), though searches of pre-explosion images are yet to find a RSG progenitor with an inferred initial mass greater than $\sim 20M_{\odot}$ (Smartt et al. 2009; Fraser et al. 2012).

In determining the bolometric luminosities of RSGs, knowledge of the temperature scale is crucial, since for the typical temperature range of RSGs ($T_{\text{eff}} \sim 3400\text{--}4500\text{K}$) the optical bolometric correction can vary by almost 2 magnitudes (Levesque et al. 2005). Therefore, in order to accurately convert the flux in a given photometric pass-band to the total flux, we must know the relationship between the star's observed properties (e.g. photometric colours, spectral type) and its T_{eff} . This

problem is complicated further by the fact that extinction A_V , whether interstellar or circumstellar, can make the star appear cooler, introducing a large degree of degeneracy between A_V and T_{eff} .

To measure the effective temperatures of RSGs, a number of different strategies have been employed, though all methods ultimately require a knowledge of the radiative transfer through the star's atmosphere. One method is to measure the angular diameters of stars through interferometry or Lunar occultations (Lee 1970; Dyck et al. 1996; Mozurkewich et al. 2003; van Belle et al. 2009). Since the definition of T_{eff} comes from $L_{\star} = 4\pi R_{\star}^2 \sigma T_{\text{eff}}^4$, where L_{\star} and R_{\star} are the stellar luminosity and radius respectively, by measuring the apparent sizes and fluxes one can determine T_{eff} .

This method does have a number of problems however. Firstly, the measured size of the star is very sensitive to the observed wavelength, with the star appearing larger in spectral regions of high opacity. For example, interferometric observations in the near-IR have shown that the apparent size of the star may increase by up to 50% around the wavelengths of strong molecular lines compared with the nearby continuum (Perrin et al. 2004;

Ohnaka et al. 2009; Tsuji 2000; Ohnaka et al. 2011; Chiavassa et al. 2010). Therefore, in order to interpret the measurements of angular diameters, model stellar atmospheres are required. Early work typically used blackbodies, which are well-known to be a poor representation of RSGs, particularly in the optical. Later work has typically used plane-parallel Kurucz models, again known to be inadequate for RSGs.

Secondly, since one needs to know the flux of the star, one also needs to know the foreground extinction. Typically it is assumed that the target star has the same foreground extinction as the other stars in its host cluster or association. However, this is likely to be an underestimate, since RSGs can produce their own circumstellar dust through their winds, providing up to a magnitude of extra visual extinction (e.g. Schuster et al. 2006; de Wit et al. 2008). A combination of these two effects could explain why near-IR angular diameter measurements provide warmer effective temperatures (i.e. smaller stellar radii) than those in the optical (van Belle et al. 2009).

Other investigations into the temperatures of RSGs have looked at their spectral energy distributions (SEDs). Dyck et al. (1974) defined a near-IR ‘colour temperature’, work which was built upon by Flower (1975, 1977). This work was however calibrated this against angular diameter measurements taken at 7100Å, which is at the centre of a deep absorption feature, and so may have over-estimated the radii. Later work fit data with synthesised spectra from plane-parallel models (White & Wing 1978; Scargle & Strecker 1979), though these models lacked detailed molecular opacities.

The most contemporary measurement of the RSG temperature scale is presented in Levesque et al. (2005, 2006, hereafter L05 and L06). These authors obtained spectrophotometry of samples of RSGs in the Galaxy and the Magellanic Clouds in the *BVRI* region of the spectrum. They then fitted this region of the spectrum, which is dominated by the TiO absorption bands which determine the spectral classification of these stars, with MARCS model atmospheres (Gustafsson et al. 2008), which are 1-D spherical hydrostatic models, important for stars with extended atmospheres. The temperature scale they found for Galactic stars was slightly warmer than was previously thought. These warmer temperatures brought Galactic RSGs into closer agreement with the predicted Hayashi limit of Geneva stellar models¹ (Meynet & Maeder 2000).

There are, however, known issues and anomalies with the L05 T_{eff} scale as well. These authors found that the temperatures derived from fitting the optical spectra were systematically offset from those expected from the $V - K$ colours, indicating that their model fits were not reproducing the correct near-IR flux. They also found a number of very cool stars in the SMC, whose temperatures were so low that they were apparently in violation of hydrostatic equilibrium (Levesque et al. 2007; Massey et al. 2007). In addition, Lançon et al. (2007) fit

¹ It should be noted that the location of the Hayashi limit in models of massive stars is governed by the convective mixing length parameter, which is typically assumed to be the same as for the Sun. Observations of globular clusters have shown that a uniform mixing length may not be appropriate for all stars, especially cool stars (Ferraro et al. 2006).

the optical and near-IR spectra of a sample of Galactic RSGs with PHOENIX models, finding problems simultaneously fitting the strengths of various molecular bands, particularly for the most luminous stars.

The reasons for these discrepancies could lie in the detailed radiative transfer that governs the strengths of the TiO bands, which are used as temperature indicators by L05 and L06. As will be discussed later, the strengths of these bands are sensitive to a number of factors, such as the temperature structure of the atmosphere and metallicity. Such factors may make the TiO bands unreliable temperature indicators.

Here we explore an alternative method of deriving the temperatures of RSGs. As in L05 and L06, we fit spectra with MARCS model atmospheres. However, in addition to looking at the strengths of the TiO bands, we also investigate the T_{eff} implied by fits to the optical-infrared SED using regions which are free of the deep molecular absorption seen in the optical regions. We do this on a sample of stars taken from the two Magellanic Clouds, which should have relatively low foreground extinction, and where the discrepancies in the Levesque et al. temperature scale appear to be most conspicuous (Levesque et al. 2007).

We begin in Sect. 2 with a description of our observations and data reduction. In Sect. 3 we discuss our analysis techniques, and present our results in Sect. 4 which indicate a systematic error in the L06 temperature scale. Reasons for this discrepancy, and possible remedies, are discussed in Sect. 5, as well as the implications of our results. We conclude in Sect. 6.

2. OBSERVATIONS & DATA REDUCTION

We have obtained observations of several stars in the LMC and SMC using VLT+XSHOOTER (D’Odorico et al. 2006) under ESO programme number 088.B-0014(A) (PI B. Davies). The sample of stars, 8 in the LMC and 10 in the SMC, were selected from L06. We aimed to sample the full distribution of spectral types observed in each galaxy. We also deliberately excluded stars which may be ‘extreme’ objects, such as analogues of the Galactic RSG VY CMa. We did so by avoiding stars which had luminosities in excess of $10^{5.5} L_{\odot}$ in L06.

The stars were observed in nodding ABBA mode with four exposures per star, and a randomized jitter at each position on the slit. For each of the instrument arms – UVB, VIS, and NIR – we used the 5.0'' slits to minimize slit losses and obtain accurate spectrophotometry. The spectral resolution was therefore set by the seeing, which for seeing of 1'' was roughly $R \equiv \lambda/\Delta\lambda \sim 5000$ at all wavelengths. The precise value of R was determined at the analysis stage (see Sect. 3). Integration times are listed in Table 1, and were chosen to achieve a signal-to-noise ratio (SNR) of at least 50 per resolution element at all wavelengths greater than 400nm. Since the UVB and VIS arms take much longer to read-out than the NIR arm, and each arm operates independently, extra time could be spent integrating in the NIR.

Flux standard stars were observed each night and to correct for the atmospheric absorption in the NIR, telluric standard stars of spectral type late-B were observed within one hour of each science target. In general observing conditions were good on each night, and the seeing was always $<1''$. The standard suite of XSHOOTER cal-

TABLE 1

OBSERVATION DATA FOR THE STARS IN OUR SAMPLE. THE ERRORS ON THE SYNTHETIC PHOTOMETRY ARE ± 0.1 MAG FOR THE OPTICAL DATA AND ± 0.04 MAG FOR THE INFRARED DATA.

Star	RA DEC (J2000)	Obs date	t_{UVB} (sec)	t_{VIS} (sec)	t_{NIR} (sec)	B	V	R	I	J	H	K_S
SMC 011709	0 48 46.32 -73 28 20.7	2011-10-13	60	10	50	14.43	12.60	11.63	10.76	9.63	8.84	8.61
SMC 013740	0 49 30.34 -73 26 49.9	2011-12-06	80	12	70	15.56	13.78	12.76	11.86	10.61	9.75	9.49
SMC 020133	0 51 29.68 -73 10 44.3	2011-12-06	60	10	50	14.84	12.86	11.76	10.73	9.39	8.56	8.27
SMC 021362	0 51 50.25 -72 05 57.2	2011-12-05	80	12	70	14.91	13.02	12.00	11.09	9.91	9.05	8.80
SMC 030616	0 54 35.90 -72 34 14.3	2011-12-06	60	10	50	14.50	12.67	11.65	10.69	9.48	8.68	8.45
SMC 034158	0 55 36.58 -72 36 23.6	2011-12-06	80	12	70	14.87	13.01	12.01	11.14	10.04	9.26	9.03
SMC 035445	0 55 58.84 -73 20 41.4	2011-12-06	100	15	100	14.59	12.91	12.00	11.20	10.09	9.31	9.09
SMC 049478	1 00 41.56 -72 10 37.0	2011-12-03	50	5	30	14.23	12.40	11.35	10.36	9.20	8.42	8.15
SMC 050840	1 01 15.99 -72 13 10.0	2011-12-06	60	10	50	14.62	12.72	11.66	10.69	9.48	8.64	8.38
SMC 057386	1 03 47.35 -72 01 16.0	2011-12-30	80	12	70	14.22	12.71	11.83	11.07	10.01	9.24	9.01
LMC 064048	5 04 41.79 -70 42 37.2	2011-12-05	60	10	50	15.09	13.15	11.94	10.69	9.42	8.55	8.19
LMC 067982	5 05 56.61 -70 35 24.0	2011-12-05	60	10	50	14.80	12.84	11.73	10.61	9.27	8.40	8.11
LMC 116895	5 19 53.34 -69 27 33.4	2011-12-06	60	10	50	14.49	12.62	11.54	10.44	9.17	8.39	8.08
LMC 131735	5 23 34.09 -69 19 07.0	2011-11-29	80	12	70	14.33	12.60	11.73	10.98	9.87	9.15	8.95
LMC 137818	5 27 14.33 -69 11 10.7	2011-11-29	60	10	50	15.34	13.38	12.03	10.65	9.34	8.52	8.18
LMC 142202	5 28 45.59 -68 58 02.3	2011-12-06	50	5	30	14.25	12.30	11.25	10.19	8.78	7.95	7.64
LMC 143877	5 29 21.10 -68 47 31.5	2011-10-13	50	5	30	14.04	12.13	11.13	10.21	9.00	8.28	8.01
LMC 158317	5 33 44.60 -67 24 16.9	2011-10-13	80	12	70	15.12	13.13	12.01	10.97	9.64	8.81	8.48

ibration frames used in the data reduction process were taken at the beginning and end of the night (for details, see Goldoni et al. 2006).

The initial steps of the reduction process were done using the XSHOOTER data reduction pipeline (Modigliani et al. 2010). These steps included subtraction of bias and dark frames, flat-fielding, order extraction and rectification, flux and wavelength calibration. The accuracy of the wavelength solution was checked by measuring the residuals of the wavelengths of the arc lines. The root-mean-square of these residuals was found to be below ~ 0.1 pixels (~ 1 km s $^{-1}$) for all targets. To check the flux calibration we applied the response function to the flux standard and compared with the calibration spectrum. We found residuals of order 1%. The absolute accuracy of the flux calibration is discussed in Sect. 2.2. When stitching the spectra of the three different arms together, we clipped the UVB arm at 563nm (to avoid the flux dropout due to the first dichroic), the VIS arm between 558-1010nm, and the NIR arm below 2350nm. The overlapping regions had consistent fluxes to within 1%, and the flux at these regions was calculated as the mean of the two overlapping spectra.

The spectra of the science targets and the telluric standards were then extracted from final rectified two-dimensional orders. The NIR spectra of the telluric standards were found to have some non-gaussian noise, mainly from bad pixels and cosmic-ray hits. To identify and remove this noise a new spectral extraction algorithm was written. Briefly, bad pixels were flagged by comparing the spatial profile at a given spectral channel with the median spatial profile of the neighbouring 3 spectral channels either side. These pixels were then replaced with the corresponding value in the median profile. Typically, around five such pixels were found and replaced per spectral order.

2.1. Telluric correction

The method of removing the telluric absorption features depended on the observing arm. For the UVB arm, telluric features are only present at the blue end of the wavelength range, where the SNR of our science data was very low due to their late spectral types. For this reason, no telluric correction was performed for the UVB arm.

In the VIS arm, telluric features are non-negligible, with prominent telluric features at 686nm, 717nm, 759nm, 815nm, and 900nm. To correct the spectra in each of these regions, we used a synthetic telluric spectrum, rather than the standard stars which have many intrinsic spectral features at these wavelengths, such as the Balmer hydrogen lines. The synthetic spectrum was optimized to best match the telluric absorption in an iterative process. In each region the relative shift of the synthetic spectrum with respect to the science data was found by cross correlation. The strength of the absorption features and effective resolution was then tuned to give the best cancellation. This whole process was then repeated.

In the NIR arm, a similar process was employed, only this time the spectrum of the telluric standard star was used. As we wish to retain flux calibration of the science data, we first flattened the telluric spectrum to remove the intrinsic continuum slope, and removed the Brackett hydrogen lines by fitting voigt profiles. The stellar continuum was corrected by fitting a black-body curve to the regions free of telluric absorption (the same regions used by the XSHOOTER pipeline in the flux-calibration step of the reduction). The temperature of the model black-body was chosen to ensure that the ratio of its spectrum to the flux-calibrated telluric standard star was closest to unity in all spectral regions tested. The accuracy of this fit was better than 5% in all tested regions of the spectrum.

The remaining spectrum, which was a pure measure of the telluric absorption, was then tuned to match the science data. To do this, the data was first split into chunks of width 10nm. For each chunk, the optimal shift, absorption strength and resolution was found as in the VIS arm. We then assumed that the absorption strength would be uniform across the whole spectrum, while the shift and resolution would vary linearly as a function of wavelength. The absorption strength at all wavelengths was taken to be the median of all those measured in each of the spectral chunks. The optimized resolution and wavelength shift as a function of wavelength were obtained from linear fits to the results from the separate spectral chunks.

2.2. Synthetic photometry

To check the accuracy of our photometric calibration, and for comparison with future and past measurements, we derived synthetic photometry for all our stars. We convolved our XSHOOTER spectra with Bessell *BVR*I filter profiles, as well as with those of the 2MASS *JHK_s* filters.

The dominant sources of error in the synthetic photometry are the accuracy of the spectrophotometric response function, and for bands which have significant telluric absorption, the quality of the telluric correction. Tests of the response function, calculated by the XSHOOTER reduction pipeline, showed that it should be accurate to a few percent, providing that the observing conditions did not change between observing the science targets and the flux standards. Similarly, imperfections in the telluric correction should only account for a few percent of the total measured flux.

To check the photometric precision and accuracy empirically, we compared our synthetic photometry with that of the Magellanic Clouds Photometric Survey (Zaritsky et al. 2002, 2004) and the 2MASS point-source catalogue (Cutri et al. 2003). Though many of the stars in our sample are known to be variable, the standard deviation of the differentials between our photometry and that in the literature can provide an upper limit to the experimental uncertainties, whilst also giving an indication of any systematics. We find that the optical *BVI* photometry has 1σ standard deviations of ± 0.2 mags, while for the 2MASS *JHK_s* photometry it is ± 0.08 mags. The systematic offsets are consistent with being zero. Given the variable nature of RSGs, which can have amplitudes $\gtrsim 0.5$ mag (e.g. Kiss et al. 2006; Levesque et al. 2007; Yang & Jiang 2012), a reasonable conservative estimate of our photometric errors is around half these values, or ± 0.1 mags for the optical data and ± 0.04 for the infrared.

3. ANALYSIS

For this study we have computed a whole new grid of model atmospheres. These atmospheres were generated using the MARCS code (Gustafsson et al. 2008), which operates under the assumptions of LTE, spherical symmetry and hydrostatic equilibrium. The grid of models is four-dimensional, computed with a range of metallicities ($\log(Z/Z_{\odot}) \equiv [Z]$), gravities ($\log g$), effective temperatures (T_{eff}) and microturbulent velocities (ξ). All model atmospheres were computed at $\xi=2$ km s⁻¹, with synthesized spectra computed at 2 km s⁻¹ and 5 km s⁻¹. The relative abundance ratios were taken from Grevesse et al. (2005). Synthetic spectra were computed from the model atmospheres using the TURBOSPECTRUM code (Alvarez & Plez 1998; Plez 2012), with a spectral resolution of $R = 500,000$ between 250-2500nm. The chemical composition was scaled from Solar at $[Z]=-1.5$ and $+0.5$ in steps of 0.25dex; T_{eff} between 3400 and 4000K in steps of 100K, with further models at 4200K and 4400K; $\log g$ between -0.5 and +1.0 in steps of 0.5 (in cgs units). All models were computed with an adopted stellar mass of $M_{\star}=15M_{\odot}$. Though RSGs may have masses between $\sim 8-25M_{\odot}$, the pressure scale height remains largely unchanged throughout this mass range (see discussion in Davies et al. 2010). Within this grid of

models, we logarithmically interpolated model spectra at metallicities appropriate for the LMC and SMC, specifically $[Z]=-0.65$ and -0.4 (Trundle et al. 2007), with models ± 0.25 dex either side of these to investigate the effect of variations in metallicity. We also logarithmically interpolated the temperatures onto a finer grid of spacing 20K.

To derive the temperatures of the stars, we employ three different techniques, and compare the results of each. Below we describe the methodology of each.

3.1. The TiO method

Firstly, we extract a region of the spectrum around the TiO bands between 500-800nm. We compare the flux in this spectral window with those of a subset of models. We initially selected models at the appropriate metallicity for the star's host galaxy (see previous section), $\log g=0.0$, and $\xi=2$ km s⁻¹. The choice of gravity is motivated by the typical masses, luminosities and radii of RSGs (see e.g. Meynet & Maeder 2000). Microturbulence parameters are typically between 2-4 km s⁻¹ (Cunha et al. 2007). In practice, varying metallicity, $\log g$ and ξ was found to have little effect on our results (see below). The parameters we are therefore allowing to vary are the temperature T_{eff} and the extinction A_V , with the latter being computed from the reddening law of Gordon et al. (2003). Broadly, T_{eff} affects the strengths of the TiO absorption, while A_V affects the overall slope of the spectrum. We find the best fitting model by computing the χ^2 summed over all spectral pixels for each value of T_{eff} and A_V . We then fit for the two parameters simultaneously by finding the model with the minimum χ^2 in $T_{\text{eff}}-A_V$ space. This method weights all TiO bands within the wavelength range equally.

The errors in T_{eff} and A_V are measured from the maximal values of those models which have χ^2 values within 0.5 of the best fitting model – this was found to be the point at which the quality of the fit becomes noticeably poorer. We also explored the best fitting models with $[Z]=\pm 0.25$ dex, with $\log g=-0.5$ – $+1.0$ dex, and with $\xi=5$ km s⁻¹. If these fits provided values of T_{eff} and A_V which were outside the errors of the initial fits, then the errors on these values were replaced by the best fits of these other subgrids. In general though, these differences were small (<50 K).

3.2. The SED method

The second method of measuring the temperatures was to apply the same technique, but to the whole of the SED *except* those regions dominated by molecular absorption, since the strengths of these bands may be sensitive to the layer at which they form in the upper atmosphere. We avoid the whole of the *BVR* spectral region, the deep absorption bands of TiO and VO, the several narrow CO bands at $\sim 1.6\mu\text{m}$ and the band-heads $>2.3\mu\text{m}$, and the CN band at $1.1\mu\text{m}$.

Before fitting, spectra were first smoothed by a box-car filter of width 10 pixels in order to wash out narrow spectral features, as it is the broad shape of the SED that we are using as a diagnostic of the temperature. As with the TiO method, we used a χ^2 -minimization technique to find the best-fitting values of T_{eff} and A_V . We again used the reddening law of Gordon et al. (2003), and explored

the effects of varying gravity, abundance and microturbulence in computing our error estimates. We also experimented with different extinction laws, specifically those of Cardelli et al. (1989) and Rieke & Lebofsky (1985), as well as values of R_V between 2-6 for the Cardelli et al. law. We found that varying the extinction law had only a very minor effect on our derived temperatures, resulting in differences to our best-fit temperatures which were less than $\pm 50\text{K}$.

3.3. The Flux Integration method

The third method uses the definition of the effective temperature,

$$\sigma T_{\text{eff}}^4 = \pi \int_0^\infty F_\lambda d\lambda \quad (1)$$

by a wavelength integral over the stellar surface flux, where σ is the Stefan-Boltzmann constant. This method takes advantage of XSHOOTER's wide wavelength range which allows to measure the effective temperature defining flux integral directly provided that the reddening and angular diameter are known. We call this method the flux integration method (FIM).

A straightforward application of the method is to assume a fixed value of interstellar reddening $E(B-V)$. In this case we can determine angular diameter and T_{eff} by a simple iterative procedure. We deredden the observed SED using the reddening law of Gordon et al. (2003), a reddening $E(B-V)$, and an initial estimate of T_{eff} , for instance the value obtained from the TiO fit. We then compare the observed flux with the model atmosphere flux at a particular wavelength (see below), and using the initial T_{eff} estimate we then calculate the angular diameter. With this angular diameter we can then turn the observed flux at all wavelengths into the stellar surface flux, calculate the flux integral, and hence a new effective temperature. The process is then iterated until the input and output temperatures converge, which usually occurs within four to five iterations.

We choose to normalise the model and observed fluxes using the wavelength range $2.17\text{-}2.20\mu\text{m}$, for the following reasons. Firstly, reddening at these wavelengths is minimal. Secondly, at these wavelengths we are close to the Rayleigh-Jeans domain of the SED. Here, one can analytically show that the process *must* converge as long as the temperature dependence of the model atmosphere flux at the wavelength λ_0 of the normalization $F_{\lambda_0}^{\text{model}} \propto T_{\text{eff}}^x$ goes with an exponent x smaller than four. Finally, the fact that the molecular line opacity at this wavelength range is weak reduces the uncertainty of the model atmosphere fluxes, and of the height in the atmosphere at which the molecules form (Perrin et al. 2004). Moreover, at these wavelengths the line and continuum form at roughly the same depth in the atmosphere as that which defines the photospheric radius in the MARCS model atmospheres.

The advantage of this method is that is only very weakly model dependent through the iterative estimate of the angular diameter at the wavelength λ_0 and that it uses directly the definition of T_{eff} . Finally, we note that this method is not new. A similar approach has been applied for hot stars (see for instance Remie & Lamers 1982) and also for cool stars (Blackwell & Shallis 1977).

TABLE 2
RESULTS FROM THE TiO AND SED METHODS OF ESTIMATING T_{eff} .

Star	T_{eff} (TiO)	A_V (TiO)	T_{eff} (SED)	A_V (SED)
	(K)		(K)	
SMC 011709	3740_{-60}^{+140}	$0.16_{-0.16}^{+0.23}$	4140_{-50}^{+50}	$0.62_{-0.10}^{+0.10}$
SMC 013740	3800_{-80}^{+260}	$0.39_{-0.16}^{+0.38}$	3920_{-50}^{+50}	$0.52_{-0.21}^{+0.10}$
SMC 020133	3640_{-60}^{+50}	$0.47_{-0.16}^{+0.15}$	4000_{-50}^{+50}	$0.93_{-0.20}^{+0.10}$
SMC 021362	3720_{-60}^{+80}	$0.31_{-0.15}^{+0.16}$	3900_{-50}^{+50}	$0.31_{-0.10}^{+0.10}$
SMC 030616	3660_{-60}^{+50}	$0.23_{-0.23}^{+0.08}$	4100_{-60}^{+50}	$0.62_{-0.10}^{+0.10}$
SMC 034158	3760_{-80}^{+120}	$0.31_{-0.15}^{+0.23}$	4100_{-50}^{+50}	$0.41_{-0.20}^{+0.11}$
SMC 035445	3860_{-100}^{+520}	$0.16_{-0.16}^{+0.61}$	4080_{-50}^{+50}	$0.41_{-0.10}^{+0.11}$
SMC 049478	3580_{-50}^{+60}	$0.16_{-0.16}^{+0.23}$	4120_{-50}^{+60}	$0.72_{-0.10}^{+0.11}$
SMC 050840	3640_{-60}^{+50}	$0.31_{-0.15}^{+0.16}$	3940_{-50}^{+50}	$0.52_{-0.21}^{+0.10}$
SMC 057386	3920_{-100}^{+460}	$0.08_{-0.08}^{+0.62}$	4040_{-50}^{+50}	$0.21_{-0.21}^{+0.10}$
LMC 064048	3520_{-60}^{+50}	$0.70_{-0.23}^{+0.23}$	3860_{-60}^{+60}	$0.62_{-0.20}^{+0.21}$
LMC 067982	3580_{-50}^{+60}	$0.47_{-0.16}^{+0.23}$	4180_{-80}^{+50}	$1.24_{-0.21}^{+0.10}$
LMC 116895	3560_{-50}^{+50}	$0.39_{-0.23}^{+0.15}$	4180_{-100}^{+60}	$0.93_{-0.31}^{+0.10}$
LMC 131735	3960_{-120}^{+320}	$0.16_{-0.16}^{+0.46}$	4360_{-60}^{+50}	$0.62_{-0.10}^{+0.10}$
LMC 136042	3460_{-50}^{+50}	$0.23_{-0.15}^{+0.31}$	4200_{-50}^{+100}	$1.65_{-0.10}^{+0.21}$
LMC 137818	3480_{-50}^{+60}	$1.08_{-0.23}^{+0.24}$	4020_{-50}^{+60}	$0.83_{-0.21}^{+0.10}$
LMC 142202	3580_{-50}^{+60}	$0.23_{-0.07}^{+0.31}$	4200_{-100}^{+50}	$1.24_{-0.21}^{+0.10}$
LMC 143877	3660_{-50}^{+60}	$0.23_{-0.15}^{+0.16}$	4360_{-60}^{+50}	$0.93_{-0.10}^{+0.10}$
LMC 158317	3640_{-60}^{+60}	$0.70_{-0.23}^{+0.15}$	4160_{-80}^{+60}	$1.24_{-0.21}^{+0.10}$

of

4. RESULTS

4.1. TiO temperatures versus SED temperatures

In Fig. 9 we show examples of the fits from the TiO and SED techniques to two of the stars in the sample. Typically, the TiO fit is excellent in the region of the TiO bands (left panels). The fitted temperatures and extinctions are in most cases consistent to within $\pm 100\text{K}$ or $\pm 0.1\text{mag}$ with those obtained by Levesque et al. (2006), who used similar models with ‘by-eye’ fitting methods. Our errors are asymmetric due to the non-linear relation between model temperature and TiO strength, while for higher TiO temperatures the errors tend to be larger, due to the diagnostic TiO bands becoming weaker. The SMC stars have less TiO absorption for a given temperature due to the reduced metal abundance. This effect explains the average spectral type of RSGs shifting to earlier subtypes in lower metallicity environments (Elias et al. 1985).

Longward of $\sim 800\text{nm}$, however, the fit is poor (right panels). Specifically, the model with the T_{eff} of the TiO fit overpredicts the flux at wavelengths greater than $\sim 900\text{nm}$, as well as a rise in flux in the H -band at $\sim 1.6\mu\text{m}$, which we call the ‘ H -hump’. It is caused by a minimum in the H^- opacity, but is suppressed at high metallicities by molecular absorption, mostly CO. We do not see the H -hump feature in our XSHOOTER data. This discrepancy is not an artifact of the fitted extinction: the grey lines in the right panels of Fig. 9 show mod-

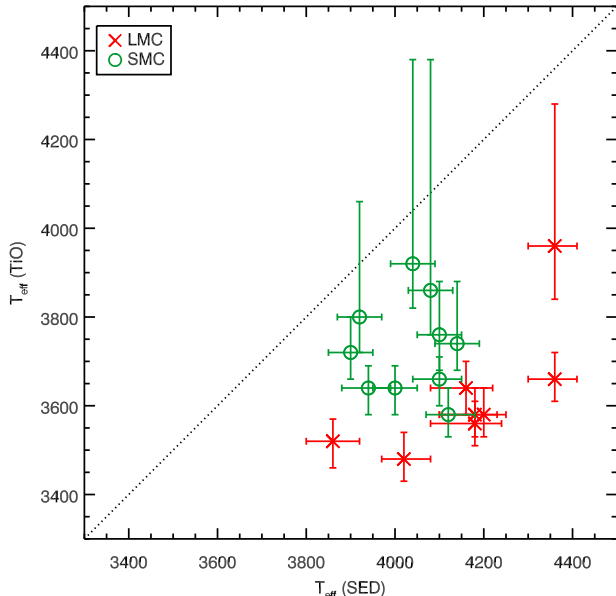


FIG. 1.— Comparison of the temperatures derived from the TiO band fits and from the SED fits.

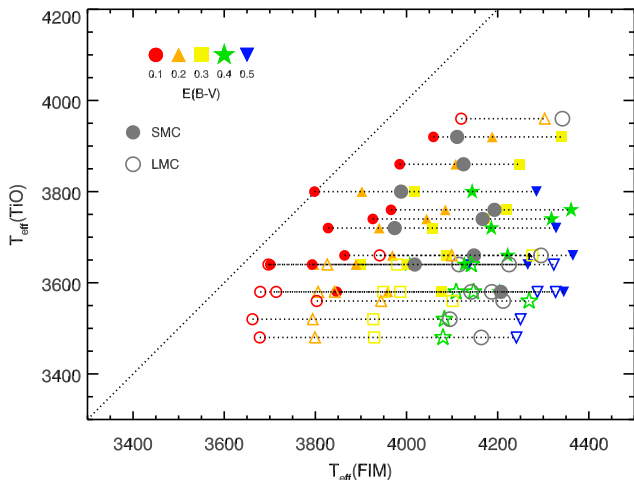


FIG. 2.— Comparison of the TiO temperatures and those from the flux integration method (FIM). The different coloured symbols represent the FIM temperature when different values of reddening were used. The grey points show the FIM fit with the lowest χ^2 value (see text for details).

els with the temperatures from the TiO fits but which have had the extinction tuned to give the best fit to the whole SED. Clearly, the fit to the NIR spectrum is still poor, due to the excess of flux around the H-hump.

In the case of the SED fits, models with higher values of T_{eff} are required to fit the NIR continuum, in which the contrast of the H-hump is reduced. This then in turn requires higher values of A_V . While the fits to the IJK region are good, the BVR region is also well matched in most cases, apart from the spectral range where the TiO features dominate ($\sim 600\text{-}800\text{nm}$). This is despite the fact that no part of the spectra blueward of 900nm was used to tune the SED fits. Only in one object is there a substantial discrepancy between the SED fit and the blue flux (LMC 137818).

To check whether the H-hump issue is an artifact of poor flux calibration, we compared the 2MASS photom-

etry of each object with our synthetic photometry computed by convolving the XSHOOTER spectra with the 2MASS filter profiles. No object has any systematic offset for the H -band flux compared with J and K_S , and the two sets of photometry agree to within the errors. Some objects do have 3σ differences in all NIR bands, though these differences are not correlated with any stellar property. We attribute these differences to photometric variability of some of the stars in our sample.

The differences in the T_{eff} values from the two fitting methods are illustrated in Fig. 1. A systematic difference in temperatures is clearly seen. In the case of the TiO fits, a systematic offset is seen between the average temperatures of the stars in the two galaxies. For the SED fits, the average T_{eff} values are roughly the same for both galaxies within the errors, $4170 \pm 170\text{K}$ and $4030 \pm 90\text{K}$ for the LMC and SMC respectively. The offset of the LMC and SMC stars in Fig. 1 is due entirely to the metallicity dependence of the TiO absorption strengths.

We note that the differences in the T_{eff} and A_V values from the two fits cannot be reconciled by changing the model metallicities, gravities or microturbulence parameters within sensible boundaries. It is possible to obtain similar results for the two analysis methods only if very high metallicities are used (i.e. $[Z] > 0.0$ for both LMC and SMC), but there is little motivation for such high abundances in the Magellanic Clouds (e.g. Trundle et al. 2007). This will be discussed further in Sect. 5.2.

As well as the SED T_{eff} values being warmer than the TiO fits, the A_V values are also higher (see Table 2). It is reasonable to ask whether these higher extinctions are believable, since unrealistically high values of A_V would put the SED T_{eff} values in doubt. In fact, these values of A_V are consistent with that of neighbouring stars, plus an extra few tenths of a magnitude for circumstellar material, consistent observations of Galactic objects (see Sect. 5.1 for further discussion).

4.2. Results from the flux integration method

In this method, the extinction A_V is unconstrained. Applying a reasonable minimum average reddening value towards the Magellanic Clouds of $E(B-V) = 0.1$ mag (Zaritsky et al. 2002, 2004) leads to a first result which is displayed as the red circles in Fig. 2. It appears that the temperatures obtained with the FIM-method for *this minimal value of reddening* are on average 200K higher than the TiO values. Note that we use the reddening laws determined by Gordon et al. (2003), which relate extinction A_V and reddening through $A_V = R_V E(B-V)$ with R_V equal to 2.7 and 3.4 in the LMC and SMC, respectively.

Of course, as already indicated by the results obtained with the SED-fitting method it is very likely the reddening and extinction towards the sites of the RSGs are much higher than the minimal reddening. To account for possible reddening values different from 0.1mag we assume a range of reddening values between $E(B-V) = 0.0\text{mag}$ and 0.5mag and determine T_{eff} in the same way as above at each reddening (orange, yellow, green and blue symbols in Fig. 2). In addition, we compare the dereddened observed fluxes with the model fluxes at three wavelength bands which are free of molecular absorption ($1.605\text{-}1.702\mu\text{m}$, $1.212\text{-}1.278\mu\text{m}$, and $1.000\text{-}1.080\mu\text{m}$) and calculate χ^2 values for each $E(B-V)$.

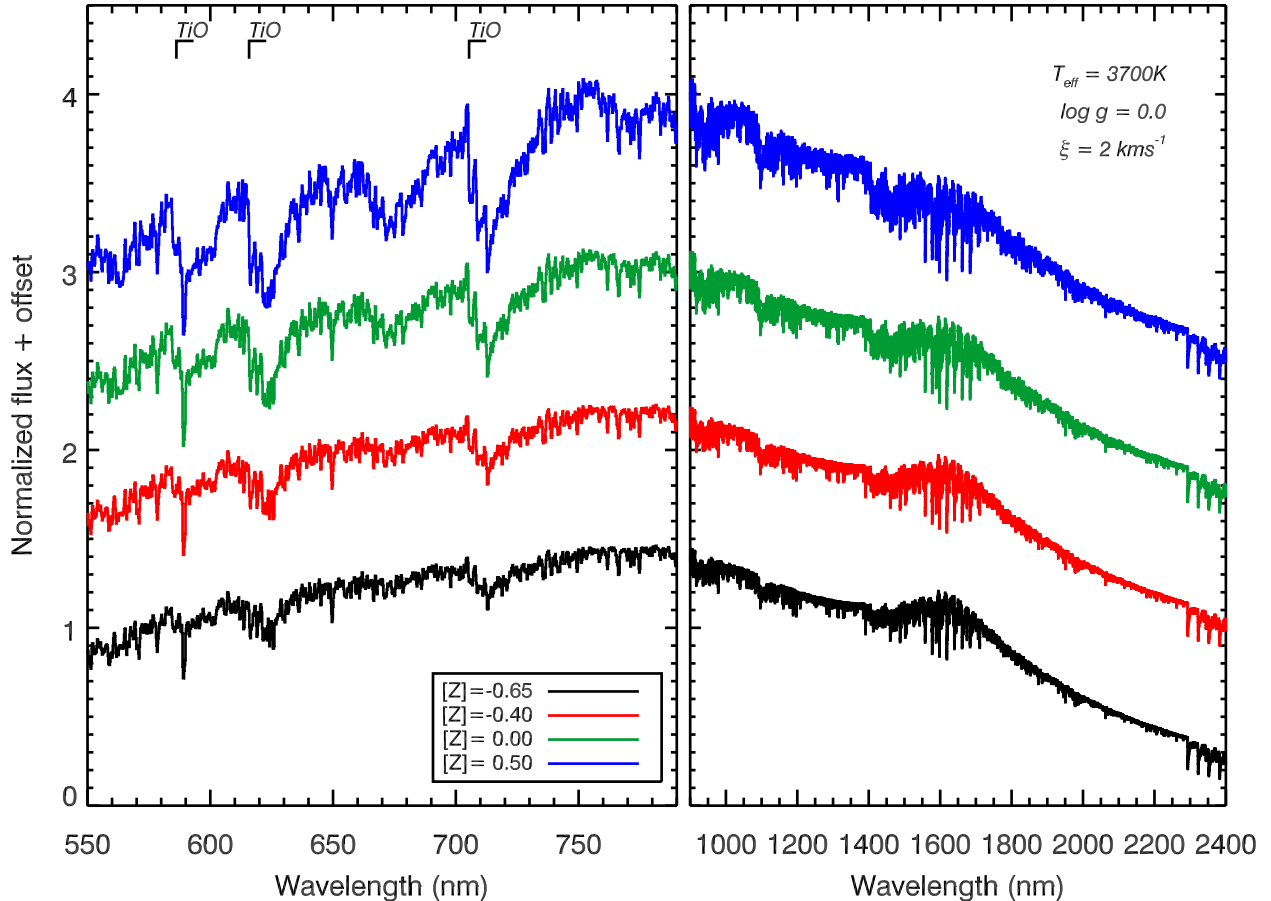


FIG. 3.— Comparison of the MARCS synthetic spectra in the regions of the TiO bands (left) and the H-hump around 1.5-1.6 μ m (right). All models have $T_{\text{eff}}=3700\text{K}$, $\log g=0.0$, and $\xi=2\text{km s}^{-1}$. The metallicities of each model are displayed in the figure legend.

The minimum of χ^2 is then used to determine the best-fitting $E(B-V)$ and T_{eff} (grey points in Fig. 2). We note that this extended method aiming at a simultaneous determination of T_{eff} and $E(B-V)$ also depends on the use of model atmospheres, and is very similar to the SED method. As such, these best-fits cannot be considered to be entirely independent of the results from the SED fits.

What these results *do* show is that, even for minimal reddening, the FIM temperatures are always higher than the TiO temperatures by 100-200K. Increasing the reddening only serves to increase the discrepancy further. We again state that deviations from the standard interstellar extinction law cannot explain this discrepancy, since this can only account for temperature differences of $\pm 50\text{K}$ even for the most extreme values of R_V . This served to cast further doubt on the reliability of the TiO temperatures.

5. DISCUSSION

5.1. Which temperature scale is correct?

Since the different fitting methods give two different temperatures for the stars observed, it is natural to ask which, if any, is correct. One major reason to be suspicious of the TiO temperatures is that they consistently overpredict the flux at wavelengths $>900\text{nm}$, dramatically so in some cases (e.g. LMC 064648, LMC 137818, see Fig. 9). Though the SED fits overpredict the *optical* flux, this may be plausibly explained by TiO absorption in the MARCS models (see later). Conversely, there is

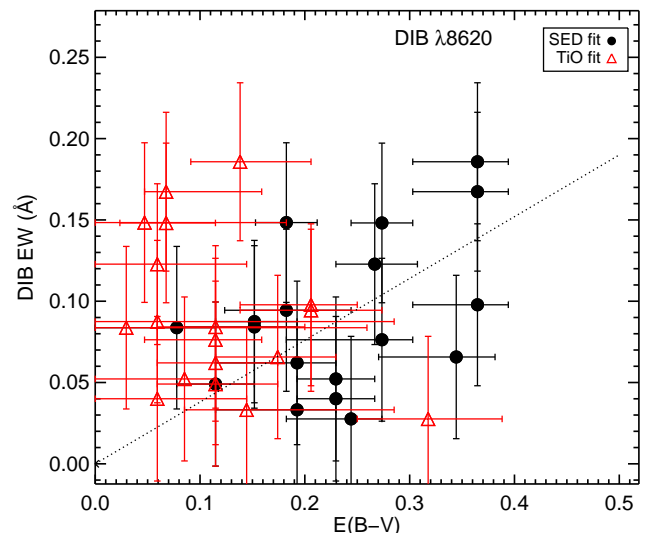


FIG. 4.— The amount of reddening deduced from each of the TiO band and SED fits, versus the equivalent width of the DIB at 8620Å. The dotted line shows the expected relation in the Galaxy, from Munari et al. (2008)

no obvious physical mechanism that would cause us to greatly overestimate the NIR flux whilst correctly matching that in the optical. One cannot reduce the extinction to rebalance the optical and NIR fluxes as the A_V values

from the TiO fits are already very low. We note that this discrepancy was already flagged in L06, who found that the $V - K$ colours of RSGs did not match the predictions of MARCS models with the same T_{eff} .

One other strong piece of evidence that the TiO temperatures are too low comes from the FIM results. This method, which uses the observed flux integrated over all wavelengths, is insensitive to model dependent features such as the predicted strengths of molecular absorption. Instead, it assumes only that the models correctly predict the ratios of the total flux to that in a specified wavelength interval, which we chose to be a small section of the K -band. These results showed that even for very low values of reddening the FIM temperatures were systematically higher than the TiO temperatures.

Another line of investigation is to examine the A_V implied by each fitting method. Here, we consider only the TiO and SED results, since the FIM results are not entirely independent of the latter. For a given fit, to some extent there will always be a degree of degeneracy between T_{eff} and A_V , since the flux peak can be shifted for example to the blue by either increasing T_{eff} or decreasing A_V ². As the two methods (TiO and SED) place emphasis on different spectral properties, each gives a different A_V . Therefore, by finding some other diagnostic of A_V , we may assess which method is providing the most reliable results.

An independent measurement of extinction may be obtained from the strengths of the diffuse interstellar bands (DIBs). Many DIBs are known to strongly correlate with reddening (e.g. Cox et al. 2006, 2007); however the majority of these features are located in the V and R bands, meaning that in RSGs they are blended with many intrinsic features. One DIB located in a relatively clean spectral region is that at 8620\AA , identified in the spectra of stars in the RAdial Velocity Experiment (RAVE) sample (Munari et al. 2008). In Fig. 4 we plot the strength of this line from each star in our sample against the reddening $E(B - V)$ obtained from each of the fitting methods. We find that the reddenings from the TiO fits appear to be poorly correlated with the DIB strengths. The formal Pearson coefficient is small and negative (-0.35), implying that if anything the data are *anticorrelated*. There is a greater degree of correlation however between the DIB strengths and the reddenings from the SED fits. This time the Pearson coefficient is positive, though still quite low (+0.44). A linear fit to the data using the GSFC IDL routine FITEXY, which considers errors in both variables³, yields a slope and offset consistent with the fit to the RAVE stars within the errors (the latter shown as a dashed line in Fig. 4). While this evidence is far from conclusive, it does provide circumstantial evidence in favour of the SED T_{eff} values over those from the TiO fits.

We can also estimate the extinction towards each star from that of the surrounding stars. Though RSGs may

² This applies mainly to the SED method, though it is also relevant to the TiO method for earlier spectral types, i.e. when the TiO bands are weak.

³ The routine assumes the errors are symmetric, whereas the errors in our $E(B - V)$ values tend to be asymmetric. However, since the level of asymmetry is small, and as we are not interested in a precise formal fit to the data, we used the larger of the two errors in this analysis.

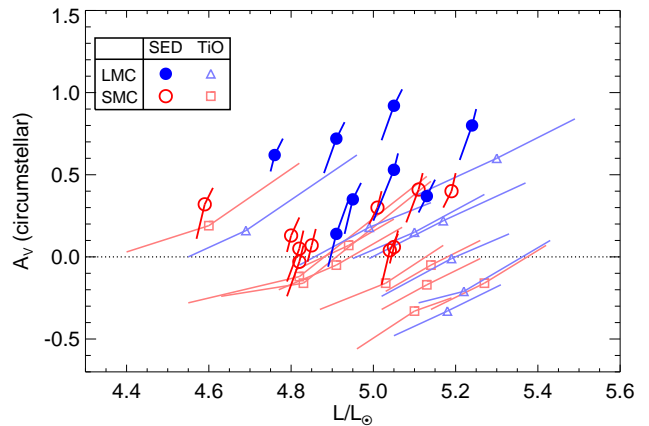


FIG. 5.— The circumstellar extinction around each star, found by subtracting the local from the total extinction, as a function of luminosity. The results of both the SED and TiO fits are shown. Note the asymmetric and correlated errors on each datapoint.

have some extra circumstellar extinction caused by their mass-loss history, the surrounding stars should give us an idea as to the foreground extinction, both Galactic and internal to the star’s host galaxy, and so give an indication as to the lower limit of the A_V towards each object.

The foreground extinction was measured by looking at that towards stars within $1'$ of our targets from Zaritsky et al. (2002, 2004). We experimented with several methods of interpolating the extinction at the location of our targets, such as binning in right-ascension and declination or in radius from the target star. In the end we found that simply median averaging the stars within $0.5'$ gave results similar to any other method tried, and was stable to within ± 0.2 mags in A_V .

In Fig. 5 we plot the circumstellar extinction (the total extinction from the spectral fits minus the foreground extinction from the neighbouring stars) as a function of stellar luminosity L (see Sect. 5.4 for details on how we measure L). The first thing to note is that the circumstellar extinction implied by the TiO fits is often negative – that is, the localized extinction is *greater* than the total extinction measured from the TiO region. In contrast, the total extinction as measured from the SED fits is always at least equal to that of the local extinction. Some objects, especially the more luminous ones, show evidence of substantial circumstellar extinction of up to $A_V = 1$ mag, consistent with mid-IR observations of Galactic RSGs (e.g. de Wit et al. 2008), and expectations calculated from simplified mass-loss histories (Walmswell & Eldridge 2012). In addition, there is a separation between the LMC and SMC stars, suggesting a possible metallicity dependence on RSG wind density.

To summarise, we conclude that the T_{eff} measurements from the strengths of the TiO lines are unreliable, since model fits to these lines overpredict the NIR flux, and extinctions implied are anomalously low. The SED temperatures on the other hand provide good fits to all parts of the spectrum apart from the TiO bands. They also imply extinctions that are consistent with their neighbouring stars with a contribution from a circumstellar component. In the following section we discuss how the mismatch between the SED and TiO results may arise, and discuss possible solutions.

5.2. Reconciling the two T_{eff} measurements

Given this clear discrepancy between the different independent temperature measurements, we now explore various explanations for this result. We first note that the differences in the T_{eff} and A_V values from the two fits cannot be reconciled by changing the model gravities or microturbulence parameters within sensible boundaries.

The discrepancy between the two methods may disappear at higher metallicities. In Fig. 3 we show the MARCS model spectra at fixed T_{eff} , $\log g$ and ξ , for SMC-like, LMC-like, Solar, and Solar+0.5dex metallicities. The strengths of the TiO bands are strongly correlated with $[Z]$, as one would expect. In addition, the strength of the H-hump is inversely correlated with $[Z]$, as atomic and molecular absorption eat away at the sub-peak caused by a minimum in the H^- opacity. These two effects may therefore act to bring the two T_{eff} measurements together: increased TiO absorption would require models with higher T_{eff} values to provide a match to TiO bands of a given strength; while a reduced H-hump would mean that good SED fits would be obtained at lower T_{eff} values. Therefore, potentially one could obtain similar results for the two analysis methods if very high metallicities are used (i.e. $[Z]>0.0$ for both LMC and SMC). However there is little motivation for such high abundances in the Magellanic Clouds. Young-age metallicity tracers such as cepheids, F supergiants and B stars consistently show average abundances of $[Z]_{\text{LMC}} = -0.4$ and $[Z]_{\text{SMC}} = -0.6$, with errors on the means of $\pm 0.05\text{dex}$, and typical intrasample dispersions of less than $\pm 0.02\text{dex}$ (e.g. Andrievsky et al. 2001; Romaniello et al. 2005; Keller & Wood 2006; Trundle et al. 2007).

5.2.1. Adjusting CNO abundances

Rather than changing the abundances of all metals in a uniform way, one might suggest that adjusting only the CNO mixture to reflect the products of nuclear burning would alter the appearance of the spectrum. The relative abundances of TiO, CN, and CO should depend on the CNO mix, and all are major sources of opacity. Altering the CNO mixture may therefore alter the temperature structure of the star, changing the strengths of the diagnostic absorption features.

To investigate this, we computed a model with $T_{\text{eff}}=3700\text{K}$, $[Z]=-0.5$, $\log g=0.0$, and $\xi=2\text{km s}^{-1}$, with a CNO mixture altered to reflect stellar evolution. Specifically, we reduced C by 0.4dex, and correspondingly increased N by +0.54dex. This is similar to the surface abundances of Galactic RSGs (Davies et al. 2009). We then compared this to a model with the same parameters other than the CNO mix set to Solar. The evolved CNO model had slightly weaker CO and CN features, due to the reduced C abundance; while TiO absorption was slightly increased due to less O being tied up in CO. However, the differences between the two were minimal. Analysing the evolved CNO model in the same way as the XSHOOTER spectra in this paper, we found that this led to T_{eff} discrepancies of less than 20K. We therefore conclude that deviations from a Solar CNO mixture cannot explain the results presented here.

5.2.2. Convection, granulation, and temperature structure

As the strengths of the TiO bands are very temperature sensitive, inadequacies in the temperature structure

of the models may lead to a discrepancy in the absorption strength as a function of T_{eff} , giving rise to the effects described in this paper. Indeed, this was suggested in L06 as an explanation for the $V - K$ discrepancy. Here we discuss possible causes of such an effect.

Convection is known to occur in the envelopes of RSGs, and is the physical justification for the inclusion of both micro- and macro-turbulence in spectral synthesis models. In order to self-consistently model these effects rather than including them in an ad-hoc fashion, one needs to switch from 1-D hydrostatic to 3-D hydrodynamic stellar models. Such work is still in its early stages, but Chiavassa et al. (2011) present a 3-D non-gray model of a RSG, along with a synthesized spectrum, and comparisons to 1-D models. These authors show that the temperature structure for the 3-D models is subtly different from that of the 1-D model, resulting in the formation zone of the TiO lines shifting outwards to larger radii and lower temperatures. In terms of the time-averaged SED of the 3-D model, they found that their non-grey model had similar TiO band strength to the 1-D model with a low $T_{\text{eff}}=3400\text{K}$, but that the SED $>1\mu\text{m}$ looked more like the 1-D model with $T_{\text{eff}}=3700\text{K}$ ⁴.

In Fig. 6 we show this quantitatively, by fitting the Chiavassa et al. <3-D> spectrum with 1D MARCS models just as in our analysis of the XSHOOTER spectra of the LMC/SMC stars. We used the same gravity and metallicity as were computed for the 3-D model ($\log g=-0.34$, $[Z]=0.0$)⁵. As with our observations, we find that the TiO fit has too much flux in the NIR, while the fitted temperature is lower than the input value ($T_{\text{TiO}} = 3580 \pm 50\text{K}$). The SED fit again provides an excellent match to all regions 500-2500nm, other than in the regions of the TiO bands, and has a temperature closer to the integrated flux of the <3-D> model ($T_{\text{SED}} = 3740 \pm 50\text{K}$). Both fitted models are discrepant at short wavelengths ($<500\text{nm}$).

Though a detailed analysis of 3-D model spectra is beyond the scope of this current work, it seems as though 3-D effects may serve to reconcile the discrepancy in the T_{eff} as measured from different regions of the spectrum we have highlighted here. In particular, the temperature in the outer layers of the 3-D model where the TiO lines form is somewhat lower, leading to increased TiO absorption. However, the temperature at optical depth $\tau \approx 1$, where the continuum forms, is roughly the same as in the 1-D model (see their Fig. 5, top-right panel). For this reason we conclude that the temperatures measured from the continuum regions are more reliable than those measured from the TiO bands.

Finally, we suggest that another potential complicating factor could be the difficulty in delineating the stellar photosphere, the molecular formation zone, and the stellar wind. If molecules form in the wind, or close to it, then their strengths may depend on wind density. If

⁴ Chiavassa et al. (2011) quote 3430K as the temperature of their model. However, this is the result of a complex non-standard averaging procedure. The integrated flux of their model corresponds to $T_{\text{eff}}=3700\text{K}$, which is also that model's temperature at $\tau = 1$.

⁵ In their paper, Chiavassa et al. (2011) state that due to the effect of convective pressure the *effective* gravity is $\log g=-0.65$. However, we found that adjusting the gravity had little effect on our fits, other than a change in the opacity below 500nm.

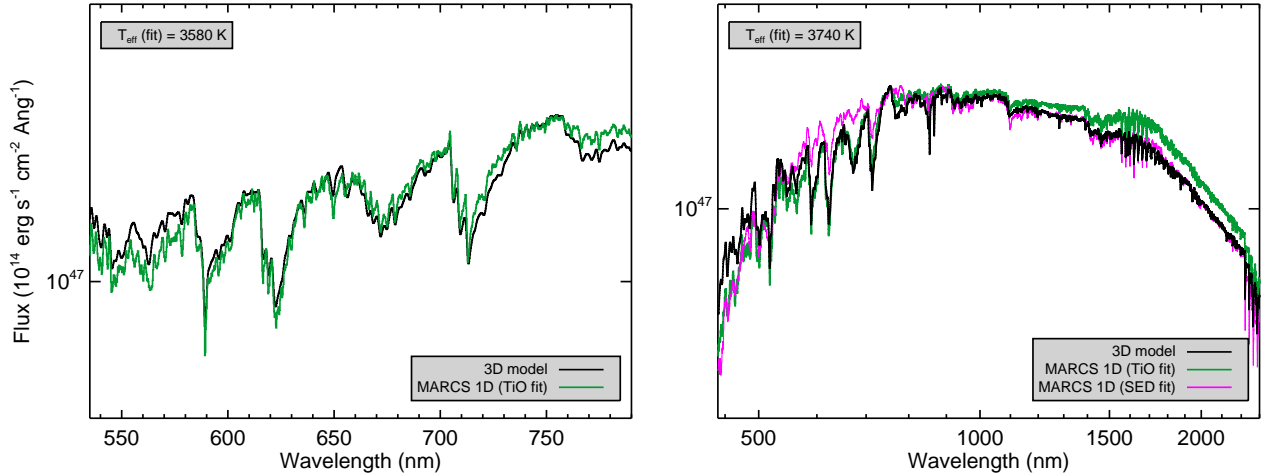


FIG. 6.— Analysis of the 3D CO⁵BOLD RSG spectrum of Chiavassa et al. (2011) with the 1D MARCS models. The left panel shows the 3D spectrum (black) along with the fit to the TiO bands (green), yielding a best-fit $T_{\text{eff}}=3600\text{K}$. The right panel shows that this fit overpredicts the flux at the H -hump, and in the K -band. Meanwhile, a fit to the NIR continuum regions (magenta) gives a higher temperature of 3800K , while underpredicting the strengths of the TiO bands. This mimics the behaviour seen in our spectra of RSGs in the Magellanic Clouds (see Fig. 9).

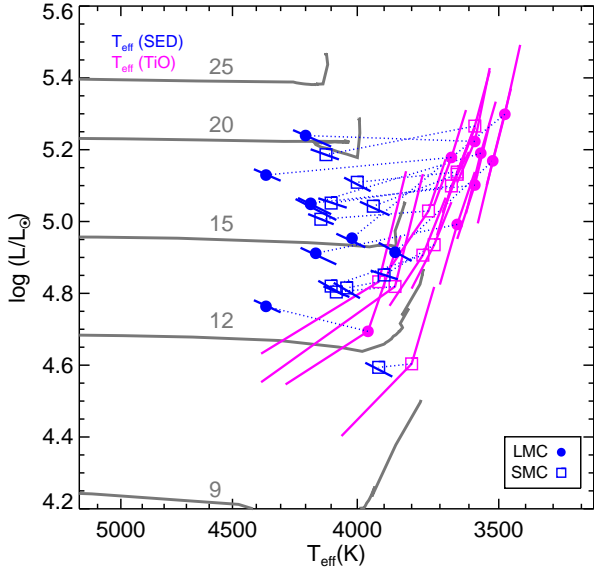


FIG. 7.— HR-diagram of the stars in our sample. The magenta points show the locations of the stars when the TiO temperatures and extinctions are used, while the blue points use the values derived from the SED fits. Note that the errors on each quantity are correlated and asymmetric. The grey lines show the Geneva mass tracks for stars with initial rotation 400 km s^{-1} and LMC-like metallicity.

the mass-loss rates of RSGs are a function of their luminosity (Bonanos et al. 2010), then the strengths of the molecular absorption bands would be highly sensitive to luminosity as well as temperature. If mass-loss rates are also $[Z]$ dependent (Mauron & Josselin 2011, see also Fig. 5 in this paper), then this may serve to increase this sensitivity of the band strengths to luminosity.

5.3. Comparison with Galactic RSGs

Since there is a known dependence of the TiO band strengths on metallicity, it is interesting to ask how a sample of Galactic RSGs would compare to the LMC and SMC stars studied here. However, obtaining data comparable to that presented here is problematic. The most

well-known Galactic RSGs, such as μ Cep and α Ori, are too bright to observe with VLT/XSHOOTER, which currently is the only instrument capable of simultaneous optical/near-IR spectrophotometry. Meanwhile, more distant RSGs such as those in the Scutum RSG clusters at 6.6 kpc (e.g. Figer et al. 2006; Davies et al. 2007) have large foreground extinction of $A_V \gtrsim 15\text{ mag}$, making optical spectrophotometry of the TiO bands extremely challenging.

We have obtained NIR spectroscopy of stars in Per OB1 with IRFT+SpeX (Gazak et al., in prep), and combined these data with the optical spectroscopy of L05. We then analysed these stars in the same way as our XSHOOTER data. We found very similar results, specifically that the SED temperatures were consistently $4100 \pm 150\text{ K}$, whereas the TiO temperatures were much cooler and varied with spectral type (agreeing well with the results of L05).

However, there are potential causes for concern with these data. Firstly they are non-contemporaneous, the optical and NIR spectroscopy taken several years apart. Secondly, the SpeX slit was $< 1''$ wide, leading to inevitable slit losses and compromising the accuracy of the spectrophotometry. Finally, the absolute photometric calibration was done with 2MASS, in which the stars are saturated and have photometric errors of $\pm 0.2\text{ mags}$. Since the data quality does not match that of our excellent XSHOOTER data, we have chosen not to present the results of that analysis here.

5.4. Implications for stellar evolution

To see how the difference in T_{eff} affects the stars' positions in the H-R diagram, we determine the luminosities of the stars for the TiO and SED T_{eff} estimates. Here, we use distance moduli of 18.47 and 18.95 for the LMC and SMC respectively (averages of a number of measurements, taken from the NASA Extragalactic Database).

For the TiO temperatures we first take the V -band magnitude of each star from our synthetic photometry. We then correct for the A_V determined from the TiO fits, and apply the bolometric corrections from L06.

For the SED fits, the luminosity was obtained by integrating under the SED. The flux in the regions of high telluric extinction was interpolated using the best-fitting MARCS model for a given star. The flux longward of $2.5\mu\text{m}$ was estimated by logarithmic interpolation between a star’s flux at $2.3\mu\text{m}$ (i.e. before the CO bandhead absorption kicks in) and the four *Spitzer*/IRAC fluxes at $3.6\mu\text{m}$, $4.5\mu\text{m}$, $5.8\mu\text{m}$ and $8.0\mu\text{m}$. The total flux outside our observed region of 400nm - $8.0\mu\text{m}$ was considered negligible. The flux was dereddened using the Gordon et al. (2003) extinction law, and assuming that the correction for wavelengths greater than $2.5\mu\text{m}$ was effectively zero. The bolometric flux was then calculated by integrating under the dereddened SED.

The H-R diagram for the stars studied here is shown in Fig. 7. When the temperatures and luminosities are updated to reflect the results of the SED analyses, we find that the stars move to warmer temperatures at roughly constant luminosity. The reason that the luminosities are largely unchanged is that, when analysing the SEDs, we find that both T_{eff} and A_V are higher than the results of the TiO fits. This means that, in the TiO fits, the smaller extinction correction is cancelled out by a larger bolometric correction.

In terms of the location of the stars in the H-R diagram in relation to the predictions of stellar evolutionary theory, the SED temperatures bring the RSGs into much better agreement with the Geneva rotating model calculations. It was pointed out by L06 that the TiO temperatures were slightly cooler than the coolest point (i.e. the Hayashi limit) of the Geneva stellar tracks. We note however that the other contemporary stellar evolution codes, such as the Bonn or Cambridge codes (Eldridge et al. 2008; Brott et al. 2011) predict that the Hayashi limit at LMC metallicity should be cooler than that of the Geneva models, at around 3700K . It is therefore worth discussing the nature of the Hayashi limit of RSGs a little further.

The Hayashi limit is the maximum size to which a star can grow whilst remaining in hydrostatic equilibrium, and depends on a number of factors, but is mainly governed by the opacity of the envelope (i.e. metallicity) and the convective mixing length parameter α (e.g. Lucy et al. 1986). In most stellar codes, α is tuned to reproduce the observed properties of the Sun, and is assumed to be the same for stars of all masses and metallicities. Some authors have argued that a single value of α cannot reproduce the colour-magnitude diagrams of globular clusters (Ferraro et al. 2006), while there is some debate about whether α may be dependent on metallicity (Salaris & Cassisi 1996; Keller 1999; Palmieri et al. 2002).

Given this discussion, it is perhaps surprising that though the Bonn, Cambridge and Geneva codes all use the same mixing length, they predict different temperatures for the Hayashi limit of RSGs. The reasons for this are unclear. The solution to this problem will ultimately come from reliable temperature measurements of RSGs. The results presented here are therefore a significant step towards understanding the nature of convection in cool stars.

5.5. Bolometric corrections, luminosity calibrations, and application to supernova progenitors

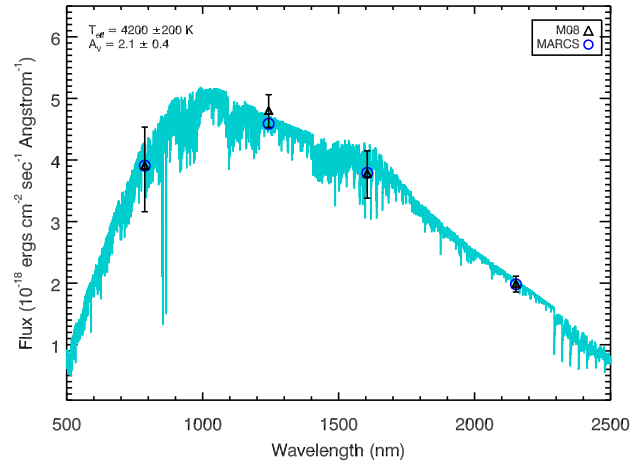


FIG. 8.— The pre-explosion photometry of SN2008bk’s progenitor, and the best-fit model with $T_{\text{eff}}=4200\text{K}$. The photometry from Mattila et al. (2008) is represented by the black triangles, while the synthetic photometry from the best-fitting MARCS model is shown by the blue circles. The full SED of that model is shown by the cyan line.

TABLE 3
MEAN BOLOMETRIC CORRECTIONS AND STANDARD DEVIATIONS FOR RSGs IN EACH OF THE TWO MAGELLANIC CLOUDS.

Galaxy	LMC	SMC
BC_K	2.69 ± 0.12	2.69 ± 0.06

TABLE 4
PARAMETERS FOR USE WITH EQ. (2) TO DERIVE BOLOMETRIC LUMINOSITIES FROM SINGLE-BAND PHOTOMETRY OF RSGs.

Band	a	b	$\sigma \log(L)$
V	3.12 ± 0.06	-0.29 ± 0.01	0.12
R	2.44 ± 0.07	-0.34 ± 0.01	0.09
I	1.90 ± 0.08	-0.37 ± 0.01	0.06
J	1.30 ± 0.09	-0.39 ± 0.01	0.03
H	0.97 ± 0.10	-0.40 ± 0.01	0.04
K	0.90 ± 0.11	-0.40 ± 0.01	0.04

5.5.1. Bolometric corrections

The uncertainties that we highlight in the RSG temperature scale are extremely important for the study of SN progenitors. Object brightnesses and colours in pre-explosion images are used to place the progenitor on the HR diagram, and by comparison with stellar models determine the progenitor mass. Clearly, such work is sensitive to both the progenitor object’s extinction and, through the bolometric correction, the calibration of colour with effective temperature.

We calculate the BC for each star in our sample from the bolometric flux, as determined from the SED fits in Sect. 5.4, the flux from the synthetic photometry (Sect. 2.2) once corrected for extinction (from the SED fits), and assuming an absolute bolometric magnitude for the Sun of 4.77.

We find that, as predicted, the BCs at various bands are correlated with temperature. However, we have shown here that the temperatures of RSGs, as determined from the continuum regions of the SED, are uniform to within $\pm 100\text{K}$. This means that the amplitude of variations in BC are small, particularly in the K -band where we are close to the flux peak and where there is little contribution from molecular absorption. Hence, to a

good approximation we can assume that for RSGs BC_K is constant to within ~ 0.1 mag.

In Table 3 we list the average BCs for the RSGs in both the LMC and SMC in the K_S band. The BCs for both galaxies are consistent with one another to within the errors. This has the important implication that we can determine the bolometric apparent magnitude of a RSG – and if the distance is known, the luminosity – from only one photometric data-point.

As is to be expected, the BC_K values presented here are much changed compared to those quoted in L06. This is caused by the incorrect assumption that the models which best-fit the TiO bands will accurately predict the flux at all wavelengths. In fact, the LMC BC_K scale is closer to that of Elias et al. (1985), which relied on averaged intrinsic colours for M supergiants and trapezoidal integration of optical/near-IR broad-band photometry. Our results for the SMC however are greatly different to those of Elias et al., since those authors did not have accurate intrinsic colours for SMC RSGs.

5.5.2. Luminosity calibrations

To be able to determine the luminosity of the star from a given photometric point, we must first measure and subtract the extinction. We separate this extinction into two components, interstellar (IS) and circumstellar (CS). The IS extinction is measured from the surrounding stars (Sect. 5.1), whereas the total (IS+CS) is measured from the SED fits. Since the CS component is typically small ($A_V \lesssim 1$), in the infrared bands this correction will be minor. Therefore, if the IS component can be estimated, one can estimate the luminosity of a RSG from K -band photometry alone. Furthermore, since the CS extinction is somewhat correlated with luminosity (see Sect. 5.1), it is possible to calibrate this effect out and estimate the luminosity from any pass-band.

To do this, we plotted the magnitudes of each star through a given pass-band, corrected for foreground extinction, against the luminosities from the SED fits. We then used the IDL procedure LINFIT to determine the coefficients of the linear fits a and b to these relations, which we list in Table 4. The bolometric luminosity of a RSG can then be determined from,

$$\log(L/L_\odot) = a + b(m_\lambda - \mu) \quad (2)$$

where m_λ is the apparent magnitude at a given pass-band *after* correction for interstellar extinction, and μ is the distance modulus. In the cases of IJK , b is close to $0.4 (=2.5^{-1})$, which follows simply from the magnitude definition. At V and R bands, b begins to diverge from this value, which is due to the flux at these bands being sensitive to CS extinction and TiO absorption, both of which are luminosity dependent. The final column of Table 4 shows the r.m.s. standard deviations of the residuals between the luminosity from the SED fits and those determined from Eq. (2). In practice, the dominant sources of error on $\log(L/L_\odot)$ are the uncertainties on a and b , which corresponds to ~ 0.1 dex at K and ~ 0.20 dex at V .

We note that we found no appreciable differences in the results when the sample was divided into stars from each of the LMC and SMC. We therefore combined all the stars to give greater signal-to-noise. In future, using

larger samples of stars, these relations could be improved upon by analysing the stars from the two galaxies separately to take account of metallicity effects, increasing the accuracy.

5.5.3. Application to pre-explosion photometry of Type II-P supernovae

To assess the potential impact on the field of SN progenitors we re-analyse the pre-explosion photometry of the Type II-P supernova 2008bk using our SED temperatures. This object was chosen as it has LMC-like metallicity, consistent with the objects studied in this current work, and pre-explosion photometry in four bands (Mattila et al. 2008), rather than the usual one or two which is the case for most progenitors (Smartt et al. 2009). In their paper, Mattila et al. fit the photometry as an M4 supergiant, $A_V = 1.0 \pm 0.5$, and using the temperature scale of Levesque et al. (2005), $BC_K = 2.9 \pm 0.1$. This led to a bolometric luminosity of $\log(L/L_\odot) = 4.6 \pm 0.1$, and by comparison to stellar models, an initial mass for the progenitor star of $9^{+4}_{-1} M_\odot$. They note that the SED may also be fit by a M0 supergiant and a higher extinction of $A_V = 3.0$.

To re-analyse the pre-explosion photometry of SN2008bk, we restrict the model T_{eff} to between 4130 ± 150 K, consistent with our results for the LMC, and use an LMC-like metallicity of $[Z] = -0.4$. We again use $\log g = 0.0$ and $\xi = 2.0 \text{ km s}^{-1}$, noting that these latter two parameters make little difference to the results. For each temperature we determine the A_V required to produce the best fit.

We find that the photometry can be fit very well by models in this temperature range, requiring an extinction of $A_V = 2.1 \pm 0.4$. Following the analysis procedure of Mattila et al. (2008), we use the object's K -band photometry ($K = 18.34 \pm 0.07$), the bolometric correction appropriate for the LMC ($BC_K = 2.69 \pm 0.12$), the extinction at K ($= A_V \times 0.11$ Rieke & Lebofsky 1985), and a distance modulus of 27.9 ± 0.2 . This gives us a bolometric luminosity for the progenitor of $\log(L/L_\odot) = 4.75 \pm 0.10$, slightly higher than the Mattila et al. (2008) estimate.

We can also estimate L_{bol} using our empirical relations in the previous section. We use the object's K -band photometry, since this is the least sensitive to extinction. Assuming negligible foreground extinction, we find $\log(L/L_\odot) = 4.72 \pm 0.14$. Mattila et al. suggest that the foreground Galactic extinction to the host galaxy is low ($A_V \sim 0.06$), but that a comparison to a SN with a similar light-curve suggests that there may be around 0.3 mag of extinction at V internal to that galaxy. This is a negligible amount of extinction at K , and would increase the luminosity of the progenitor by only ~ 0.01 dex.

To convert this luminosity into an initial stellar mass, we compare to the stellar evolutionary tracks at LMC metallicity. We use the tracks of both the Bonn (Brott et al. 2011) and Geneva groups. Our assumed temperature for the progenitor star means that its location in the HR-diagram does not coincide with the terminal point of any of these tracks, which evolve to temperatures of ~ 3500 K. However, as noted earlier, this terminal T_{eff} is set by the adopted value for the mixing length in the stellar structure models, which is poorly constrained for massive stars. In order to estimate the initial mass of the progenitor, we follow the methodology

of Smartt et al. (2009, and references therein) and compare the star’s luminosity to the terminal luminosities of the mass tracks, which corresponds to the luminosity at the end of He burning. In this way, we find a progenitor mass for SN2008bk of $M = 12^{+2}_{-1} M_{\odot}$ using the Bonn tracks, and $M = 11 \pm 1 M_{\odot}$ with Geneva tracks. This is $\sim 30\%$ higher than the previous estimate of Mattila et al. (2008), though within their errors.

We note that our extinction is slightly higher than that derived by Mattila et al. (2008), and that those authors argued against a higher A_V solution due to the lack of signs of circumstellar extinction in the SN spectrum. However, it is entirely plausible that for a relatively small amount of circumstellar extinction close to the star, this material would be destroyed almost instantly by the SN explosion. Indeed, Fraser et al. (2012) make a similar argument for the progenitor of SN2012aw, for which multi-band pre-explosion photometry was also available.

In summary, we find that if we take the temperatures of RSGs as derived from fits to the near-IR SED, the extinction increases, while the magnitude of the bolometric correction decreases. Though these two effects work in opposite directions, in the case of SN2008bk the net effect is for the progenitor star’s inferred bolometric luminosity to increase by 0.14dex. Therefore, the initial mass of the progenitor is higher compared to that derived using the Levesque et al. (2005, 2006) temperature scale. If the change in temperature scale affects the properties of progenitors in the same way, this may in part explain the so-called ‘Red Supergiant problem’ (Smartt et al. 2009), whereby the progenitor masses of Type II-P SNe tend to be lower than those expected from initial mass function arguments. This is similar to the suggestion of Walmswell & Eldridge (2012) that the ‘missing’ SN progenitors could be RSGs which have sufficient circumstellar extinction to push them below the detection limits of the pre-explosion imaging.

5.6. Concluding remarks on the temperatures of Red Supergiants

In the course of this work, we have shown that for RSGs the definition of a characteristic temperature is a non-trivial task. The definition of effective temperature, $T_{\text{eff}} \equiv L/(4\pi R^2\sigma)$, whilst unambiguous for stars such as the Sun with well-defined photospheres, can be problematic to define for stars with extended atmospheres. Simply defining the photosphere to be where the optical depth $\tau = 2/3$ is insufficient, since this value can be reached at very different radii depending on the observed wavelength. Any flux-averaged value of τ will therefore be sensitive radiative transfer processes in the stellar atmosphere.

Another problem is finding accurate and robust spectral diagnostics of T_{eff} . For M supergiants, it has always been assumed that the strengths of the TiO bands, which define the spectral classification sequence of these stars, were useful diagnostics of effective temperature. However, any diagnostic line is sensitive *only* to the local temperature in the layers where the line forms. In the case of the TiO lines, these form high in the atmosphere, and so are very sensitive to the radial temperature structure. As we have shown in our comparison to 3-D hydrodynamic models, two stars with the same luminosity and radius can have different TiO strengths if the tem-

perature structure is different. However the continuum, which forms at much deeper layers, is indistinguishable. Though there is potentially a degeneracy with reddening, this degeneracy can be broken by considering the magnitude of the H^- opacity minimum. We therefore conclude that the most robust diagnostic of T_{eff} in RSGs is the line-free continuum in the *IJK* region, including the *H*-hump.

5.6.1. A connection between spectral type and evolutionary stage?

Finally, it is worth posing the question that if the temperatures of RSGs are all roughly constant, what is the physical interpretation of the spectral type sequence? It has long since been assumed that the MK classification system was associated with a decreasing temperature scale from O to M types, with the subtypes from late-K onwards being determined from the strengths of the TiO bands. This assumption may well be valid for M giants and dwarfs, in which the pressure scale-heights and convective cells are much smaller with respect to the size of the star. However, in the case of RSGs, our results from SED fitting show that the temperatures are not strongly correlated with the strengths of the TiO bands (and therefore spectral type). Inspection of Fig. 7 reveals that the T_{TiO} values (a proxy for spectral type) do seem to be correlated with *luminosity*, similar to the Ca II lines used in extragalactic studies (e.g. Humphreys et al. 1986). Therefore, in the M supergiant domain, it seems the spectral types of stars are highly sensitive to luminosity as well as temperature.

In discussing this further, we first make the assumption that the TiO lines, which form far above the continuum-forming layers, are sensitive to the star’s pressure scale-height h . This parameter goes as $h \sim T/g$, from which it is trivial to show that $h \sim L/T^3$, or if normalised to the size of the star, $h/R \sim L^{0.5}/T$ (assuming constant mass). Even using the previous temperature scale of L05, the range in temperatures of RSGs is quite narrow, $\sim 3600\text{--}4400\text{K}$ (or $\pm 10\%$). By contrast, evolutionary models show that one expects a RSG to increase in L by a factor of ~ 2 as it evolves (see e.g. Fig. 8 in Meynet & Maeder 2000). Therefore, as a star ascends the RSG branch, its scale-height will increase, driven primarily by the increasing luminosity.

From this we suggest that RSGs with the earliest spectral types may be those objects which have just arrived in the RSG phase, having evolved from the blue. The time-averaged spectral type of a RSG will then move steadily to later types as the star gradually increases in luminosity as it evolves. This is consistent with observations of coeval clusters of RSGs, where all RSGs should have approximately the same initial mass, in which a correlation is found between MK spectral type and mid-IR excess (Cohen & Gaustad 1973). Larger excess emission is indicative of larger amounts of circumstellar material, which suggests higher mass-loss rates (associated with higher luminosity, and hence more evolved objects), and/or a star which has spent longer in the RSG phase.

5.6.2. Future work

In the present study, we have highlighted the differences and similarities between the synthesised spectra of 1-D and 3-D models. Concentrating on these similarities,

we have redefined the temperatures of RSGs using the 1-D models, and provided results which should be robust to 3-D effects. In the future we intend to make a more thorough analysis of this by repeating this study with a grid of 3-D models. The switch from 1-D hydrostatic to 3-D hydrodynamic models is non-trivial as it requires a dramatic increase in computational effort, nevertheless work is currently underway to construct such a grid.

With a suite of 3-D models we will also address the effect of any departures from spherical symmetry. Should the surface flux of the star be non-uniform, e.g. due to hot-spots and cool-spots, the relation of Eq. (1) would no longer hold. This would then cause the observer to underestimate the size of the star for a given temperature and bolometric flux. This is important with respect to comparisons with evolutionary models, which compute an effective temperature from the size and luminosity of a star assuming spherical symmetry.

6. SUMMARY & CONCLUSIONS

We have re-appraised the temperatures of Red Supergiants (RSGs) in the Magellanic Clouds using XSHOOTER flux-calibrated spectroscopy from 400-2500nm. We simultaneously fit effective temperature T_{eff} and extinction A_V by fitting the spectra with a grid of 1-D spherical MARCS model atmospheres.

When fitting the *VRI* spectral region, which is dominated by the TiO absorption which has historically been used to define these stars' temperatures, we find temperatures much lower than from fitting the continuum SED in the *IJK* region. After exploring many avenues of evidence, we conclude that the SED temperatures are the more reliable, for the following reasons:

- Models which are tuned to match the TiO bands overpredict the flux longward of $\sim 900\text{nm}$, dramatically so in some cases. The SED fits on the other hand provide good to all regions of the spectrum, apart from the regions where the TiO bands dominate.
- The TiO temperatures T_{TiO} are lower than those measured from comparing the integrated fluxes of the data with those of models (the *flux integration method*, *FIM*), which is the least model-dependent method of determining temperature. Even if we assume minimal reddening, the FIM temperatures T_{FIM} are higher than those from the TiO fits. The FIM temperatures do agree with the SED fits if we assume a modest amount of extinction, an entirely reasonable assumption.
- The implied total line-of-sight extinctions from the TiO fits are in most cases *lower* than those of nearby stars, even though RSGs are expected to have higher extinction due to circumstellar material. By contrast, the SED fits imply extinctions which are in agreement with or in excess of that of the nearby stars.
- The extinction from the TiO fits seems to be completely uncorrelated with the strengths of the diffuse interstellar band at 862nm, whereas the extinction from the SED fits appears to show a degree of correlation.

To reconcile these two measurements of temperature, we considered the effects of overall metallicity, CNO mixture, and dynamical effects (convection and granulation). Of these we conclude that the latter is most likely cause. Recent studies have shown that 3-D hydrodynamical models of RSGs have a significantly different radial temperature profile in the upper layers of the atmosphere where the TiO lines form. The temperature structure at deeper layers, where the continuum forms, is largely unchanged. For this reason we consider the *IJK* continuum region and the H^- opacity minimum at $1.6\mu\text{m}$ to be robust temperature indicators.

Adopting the SED temperatures, we find a number of interesting effects. Firstly, the temperatures of all RSGs in both Magellanic Clouds are roughly uniform, $4150 \pm 150\text{K}$. This brings the observed Hayashi limit for massive stars into agreement with those of Geneva models, and somewhat warmer than those of Bonn and Cambridge models. This also means that the strengths of the TiO bands, which define the spectral types of M supergiants, may also strongly depend on luminosity. From this we suggest that the spectral type of a RSG may be indicative of its evolutionary state, with more evolved RSGs having later spectral types.

Secondly, the circumstellar extinction of RSGs is weakly correlated with luminosity, consistent with recent findings that more luminous stars have stronger winds. We also see a separation between LMC and SMC stars, implying a metallicity dependence on wind strength.

Thirdly, as there is very little variation in temperature of the RSGs, their bolometric corrections are all approximately the same. This means that, if we can account for extinction, we can determine a RSG's bolometric luminosity to a high degree of precision from a single photometric point. This has applications for the study of supernova progenitors, where pre-explosion imaging is often limited to one or two photometric bands. We have shown that the circumstellar extinction is very low in the near-infrared, so if the foreground extinction is known (e.g. from neighbouring stars) the luminosity can be measured to a precision of $\pm 0.1\text{dex}$ from only one photometric band. In the optical (*VRI*) region, circumstellar extinction becomes more significant, as does the effect of TiO absorption on the broad-band flux. However, since both these effects are luminosity dependent, we have been able to provide a calibration which recovers the luminosity from optical photometry to a precision of $\pm 0.2\text{dex}$.

Acknowledgments: BD is supported by a fellowship from the Royal Astronomical Society. The data used in this paper is from ESO programme 088.B-0014(A). This work was supported in part by the National Science Foundation under grant AST-1108906 to RPK. Moreover, RPK acknowledges support by the Alexander-von-Humboldt Foundation and the hospitality of the Max-Planck-Institute for Astrophysics in Garching and the University Observatory Munich, where part of this work was carried out. For our analysis we used the software package IDL, the The IDL Astronomy User's Library at GSFC, and the Coyote graphics library. Finally, we thank Sylvia Ekstrom, John Eldridge, Roberta Humphreys, Norbert Langer, Emily Levesque, Phil

Massey, Georges Meynet, and Chris Tout for useful discussions.

7. APPENDIX

REFERENCES

- Alvarez, R., & Plez, B. 1998, *A&A*, 330, 1109
 Andrievsky, S. M., Kovtyukh, V. V., Korotin, S. A., Spite, M., & Spite, F. 2001, *A&A*, 367, 605
 Blackwell, D. E., & Shallis, M. J. 1977, *MNRAS*, 180, 177
 Bonanos, A. Z., Lennon, D. J., Köhlinger, F., et al. 2010, *AJ*, 140, 416
 Brott, I., de Mink, S. E., Cantiello, M., et al. 2011, *A&A*, 530, A115+
 Cardelli, J. A., Clayton, G. C., & Mathis, J. S. 1989, *ApJ*, 345, 245
 Chiavassa, A., Collet, R., Casagrande, L., & Asplund, M. 2010, *A&A*, 524, A93
 Chiavassa, A., Freytag, B., Masseron, T., & Plez, B. 2011, *A&A*, 535, A22
 Cohen, M., & Gaustad, J. E. 1973, *ApJ*, 186, L131
 Cox, N. L. J., Cordiner, M. A., Cami, J., et al. 2006, *A&A*, 447, 991
 Cox, N. L. J., Cordiner, M. A., Ehrenfreund, P., et al. 2007, *A&A*, 470, 941
 Cunha, K., Sellgren, K., Smith, V. V., et al. 2007, *ApJ*, 669, 1011
 Cutri, R. M., Skrutskie, M. F., van Dyk, S., et al. 2003, 2MASS All Sky Catalog of point sources. (The IRSA 2MASS All-Sky Point Source Catalog, NASA/IPAC Infrared Science Archive. <http://irsa.ipac.caltech.edu/applications/Gator/>)
 Davies, B., Figer, D. F., Kudritzki, R.-P., et al. 2007, *ApJ*, 671, 781
 Davies, B., Kudritzki, R., & Figer, D. F. 2010, *MNRAS*, 407, 1203
 Davies, B., Origlia, L., Kudritzki, R., et al. 2009, *ApJ*, 696, 2014
 de Wit, W. J., Oudmaijer, R. D., Fujiyoshi, T., et al. 2008, *ApJ*, 685, L75
 D’Odorico, S., Dekker, H., Mazzoleni, R., et al. 2006, in Society of Photo-Optical Instrumentation Engineers (SPIE) Conference Series, Vol. 6269, Society of Photo-Optical Instrumentation Engineers (SPIE) Conference Series
 Dyck, H. M., Benson, J. A., van Belle, G. T., & Ridgway, S. T. 1996, *AJ*, 111, 1705
 Dyck, H. M., Lockwood, G. W., & Capps, R. W. 1974, *ApJ*, 189, 89
 Eldridge, J. J., Izzard, R. G., & Tout, C. A. 2008, *MNRAS*, 384, 1109
 Elias, J. H., Frogel, J. A., & Humphreys, R. M. 1985, *ApJS*, 57, 91
 Ferraro, F. R., Valenti, E., Straniero, O., & Origlia, L. 2006, *ApJ*, 642, 225
 Figer, D. F., MacKenty, J. W., Robberto, M., et al. 2006, *ApJ*, 643, 1166
 Flower, P. J. 1975, *A&A*, 41, 391
 —. 1977, *A&A*, 54, 31
 Fraser, M., Maund, J. R., Smartt, S. J., et al. 2012, ArXiv e-prints
 Goldoni, P., Royer, F., François, P., et al. 2006, in Society of Photo-Optical Instrumentation Engineers (SPIE) Conference Series, Vol. 6269, Society of Photo-Optical Instrumentation Engineers (SPIE) Conference Series
 Gordon, K. D., Clayton, G. C., Misselt, K. A., Landolt, A. U., & Wolff, M. J. 2003, *ApJ*, 594, 279
 Grevesse, N., Asplund, M., & Sauval, A. J. 2005, in *EAS Publications Series*, Vol. 17, *EAS Publications Series*, ed. G. Alecian, O. Richard, & S. Vauclair, 21–30
 Gustafsson, B., Edvardsson, B., Eriksson, K., et al. 2008, *A&A*, 486, 951
 Humphreys, R. M., Aaronson, M., Lebofsky, M., et al. 1986, *AJ*, 91, 808
 Humphreys, R. M., & Davidson, K. 1979, *ApJ*, 232, 409
 Keller, S. C. 1999, *AJ*, 118, 889
 Keller, S. C., & Wood, P. R. 2006, *ApJ*, 642, 834
 Kiss, L. L., Szabó, G. M., & Bedding, T. R. 2006, *MNRAS*, 372, 1721
 Lançon, A., Hauschildt, P. H., Ladjal, D., & Mouhcine, M. 2007, *A&A*, 468, 205
 Lee, T. A. 1970, *ApJ*, 162, 217
 Levesque, E. M., Massey, P., Olsen, K. A. G., & Plez, B. 2007, *ApJ*, 667, 202
 Levesque, E. M., Massey, P., Olsen, K. A. G., et al. 2005, *ApJ*, 628, 973
 —. 2006, *ApJ*, 645, 1102
 Lucy, L. B., Robertson, J. A., & Sharp, C. M. 1986, *A&A*, 154, 267
 Massey, P., Levesque, E. M., Olsen, K. A. G., Plez, B., & Skiff, B. A. 2007, *ApJ*, 660, 301
 Mattila, S., Smartt, S. J., Eldridge, J. J., et al. 2008, *ApJ*, 688, L91
 Maun, N., & Josselin, E. 2011, *A&A*, 526, A156
 Meynet, G., & Maeder, A. 2000, *A&A*, 361, 101
 Modigliani, A., Goldoni, P., Royer, F., et al. 2010, in Society of Photo-Optical Instrumentation Engineers (SPIE) Conference Series, Vol. 7737, Society of Photo-Optical Instrumentation Engineers (SPIE) Conference Series
 Mozurkewich, D., Armstrong, J. T., Hindsley, R. B., et al. 2003, *AJ*, 126, 2502
 Munari, U., Tomasella, L., Fiorucci, M., et al. 2008, *A&A*, 488, 969
 Ohnaka, K., Hofmann, K.-H., Benisty, M., et al. 2009, *A&A*, 503, 183
 Ohnaka, K., Weigelt, G., Millour, F., et al. 2011, *A&A*, 529, A163
 Palmieri, R., Piotto, G., Saviane, I., Girardi, L., & Castellani, V. 2002, *A&A*, 392, 115
 Perrin, G., Ridgway, S. T., Coudé du Foresto, V., et al. 2004, *A&A*, 418, 675
 Plez, B. 2012, *Astrophysics Source Code Library*, 5004
 Remie, H., & Lamers, H. J. G. L. M. 1982, *A&A*, 105, 85
 Rieke, G. H., & Lebofsky, M. J. 1985, *ApJ*, 288, 618
 Romaniello, M., Primas, F., Mottini, M., et al. 2005, *A&A*, 429, L37
 Salaris, M., & Cassisi, S. 1996, *A&A*, 305, 858
 Scargle, J. D., & Strecker, D. W. 1979, *ApJ*, 228, 838
 Schuster, M. T., Humphreys, R. M., & Marengo, M. 2006, *AJ*, 131, 603
 Smartt, S. J., Eldridge, J. J., Crockett, R. M., & Maund, J. R. 2009, *MNRAS*, 395, 1409
 Trundle, C., Dufton, P. L., Hunter, I., et al. 2007, *A&A*, 471, 625
 Tsuji, T. 2000, *ApJ*, 538, 801
 van Belle, G. T., Creech-Eakman, M. J., & Hart, A. 2009, *MNRAS*, 394, 1925
 Walmswell, J. J., & Eldridge, J. J. 2012, *MNRAS*, 419, 2054
 White, N. M., & Wing, R. F. 1978, *ApJ*, 222, 209
 Yang, M., & Jiang, B. W. 2012, *ApJ*, 754, 35
 Zaritsky, D., Harris, J., Thompson, I. B., & Grebel, E. K. 2004, *AJ*, 128, 1606
 Zaritsky, D., Harris, J., Thompson, I. B., Grebel, E. K., & Massey, P. 2002, *AJ*, 123, 855

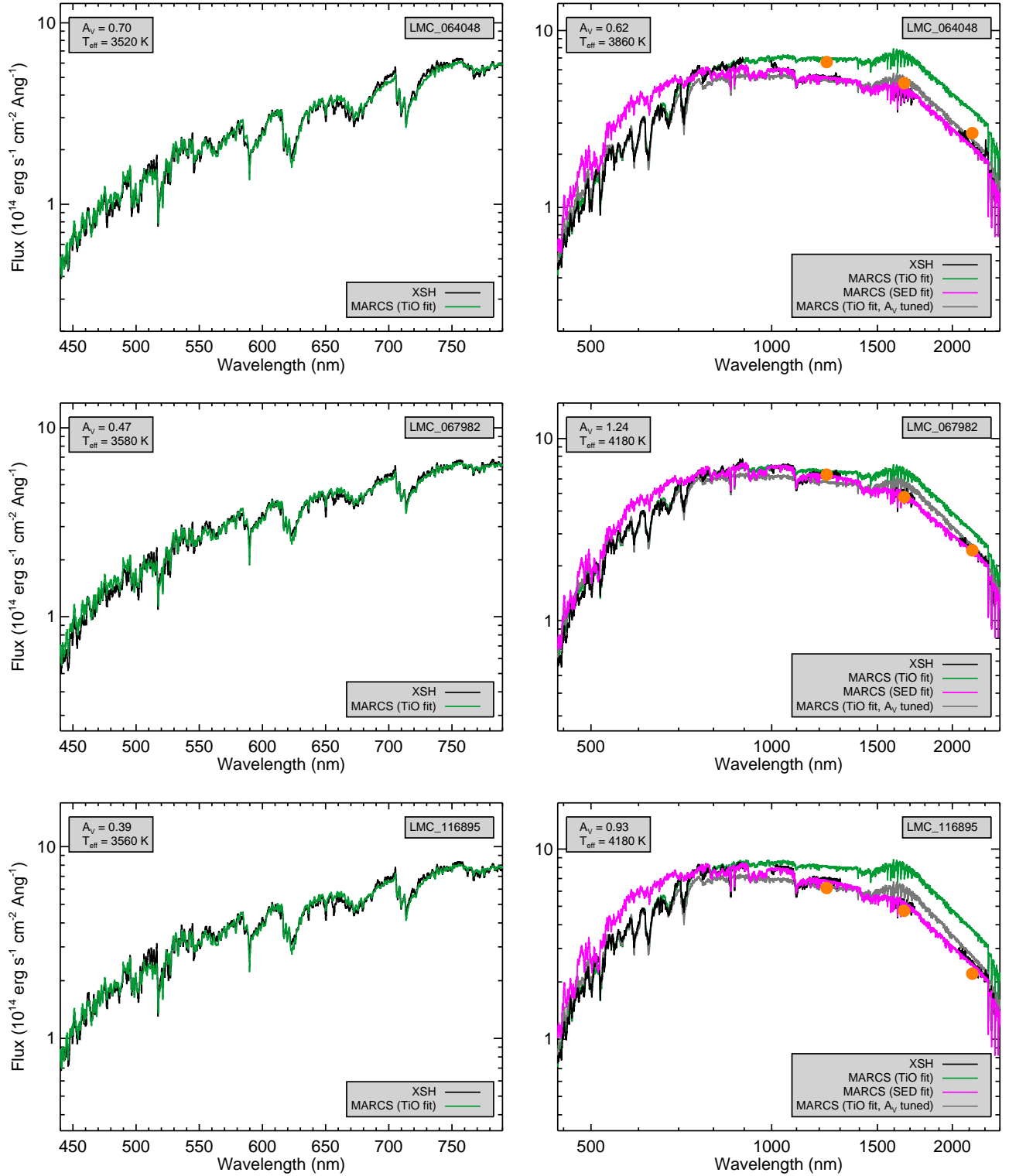


FIG. 9.— MARCS model fits to the XSHOOTER data. The left panels show the observations (black) and the best fitting model (green), along with the fit parameters in the top right. The right panels show the same data over a broader wavelength range (black), the best SED fit (magenta), the TiO bands fit from the left panel (green), and the best fitting model with the T_{eff} from the TiO bands fit but which has had the extinction tuned in order to give the best fit to the whole SED (grey). Overplotted in orange are the 2MASS photometry for each star.

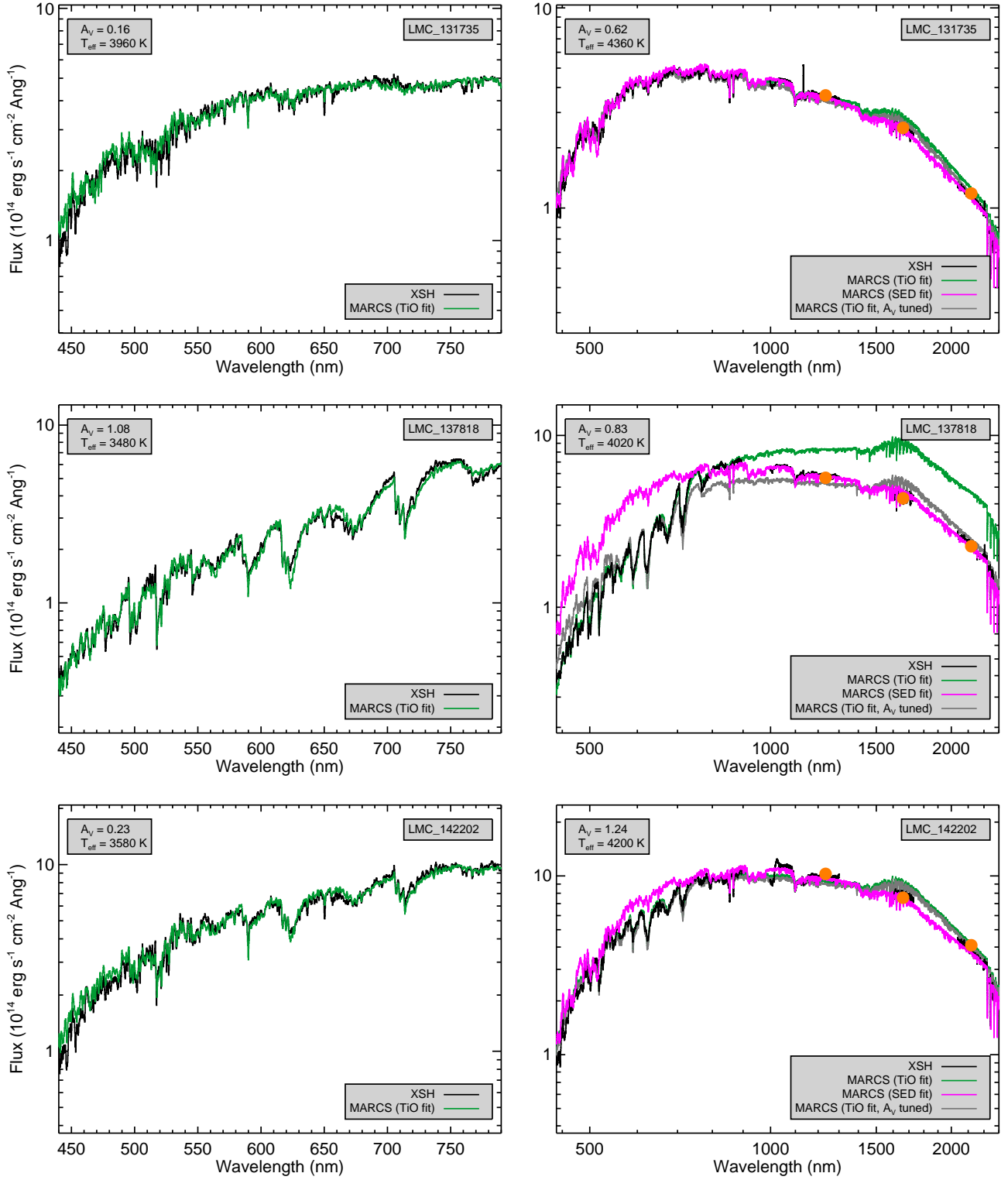


FIG. 9.— Continued.

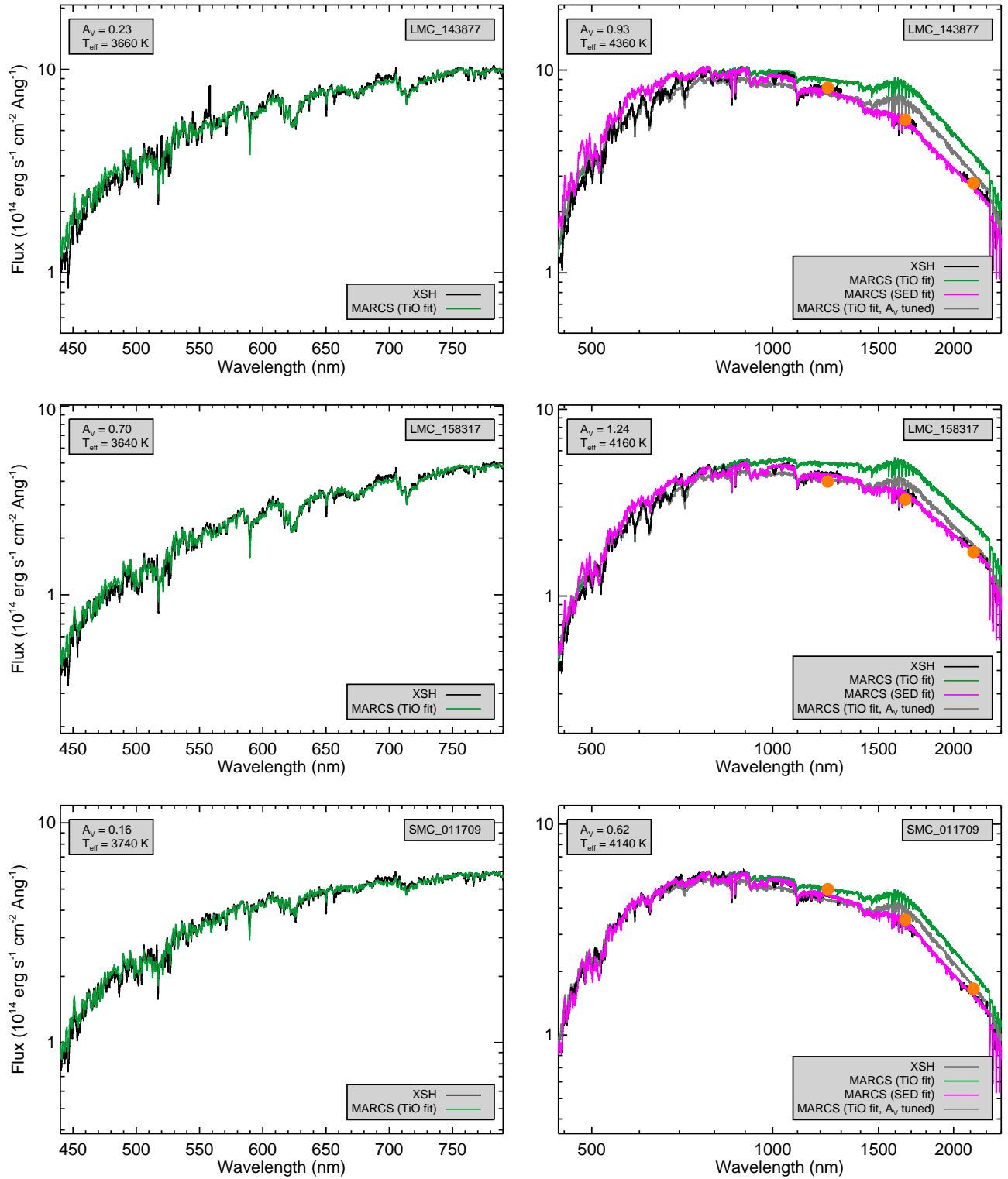


FIG. 9.— Continued.

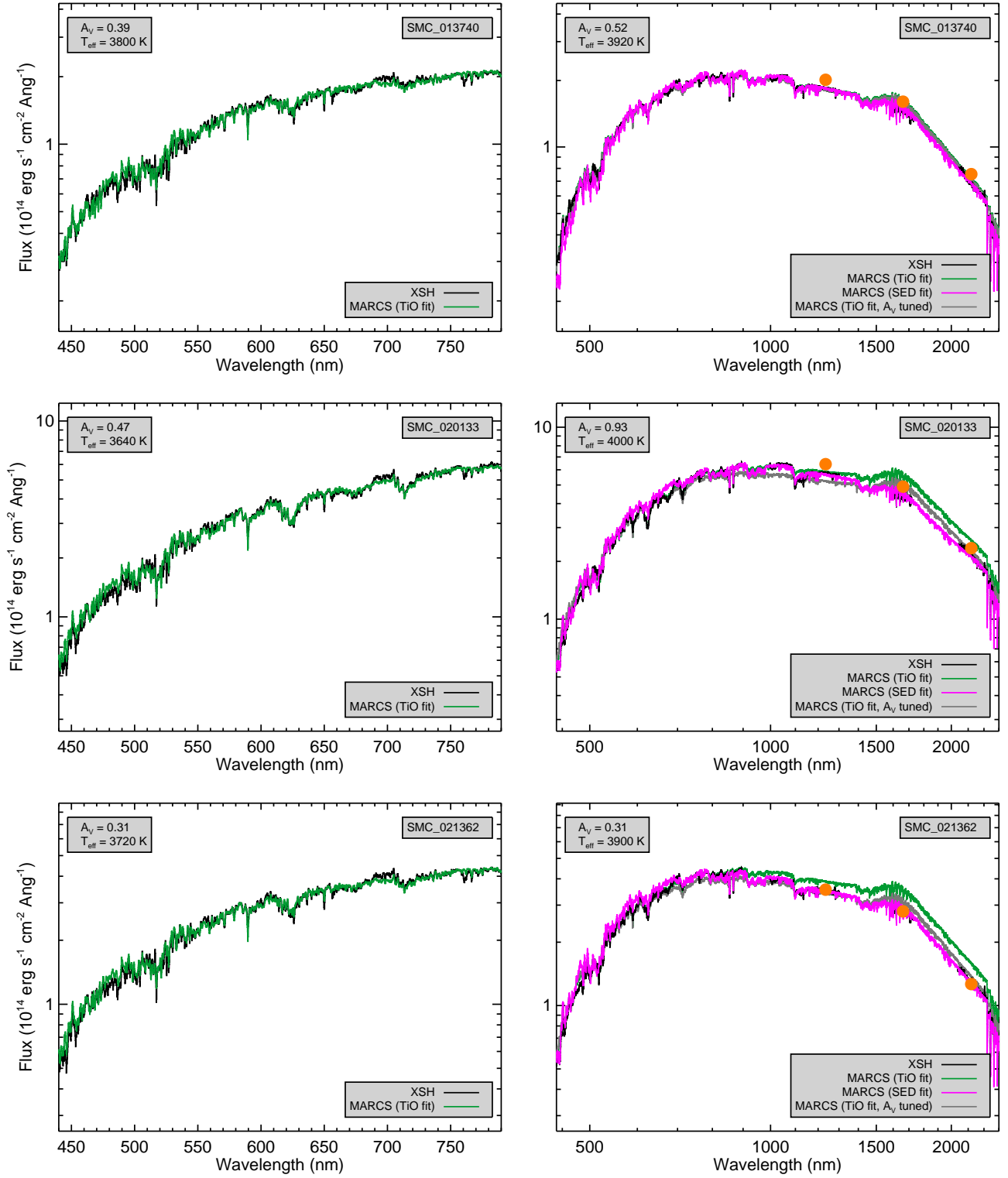


FIG. 9.— Continued.

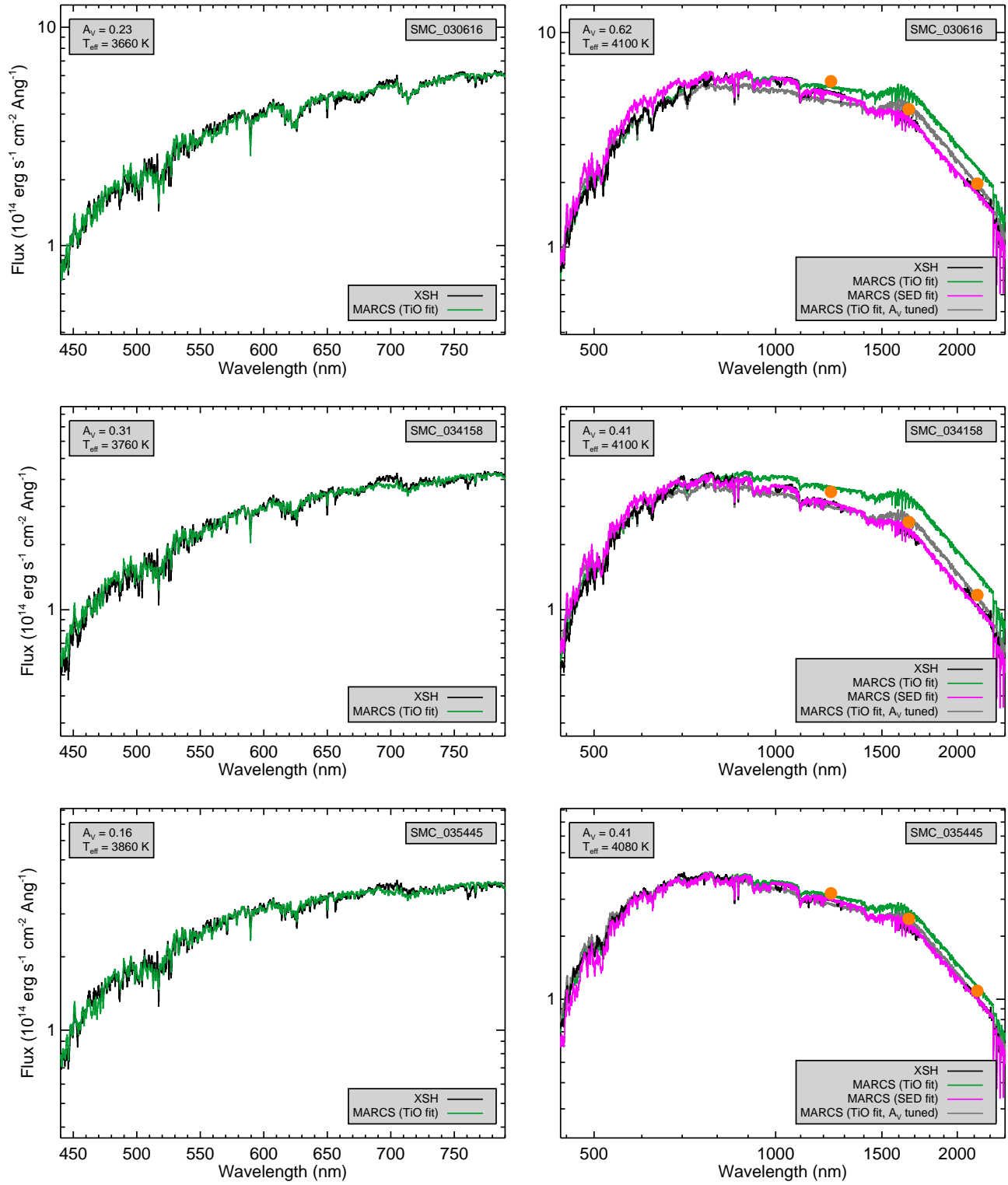


FIG. 9.— Continued.

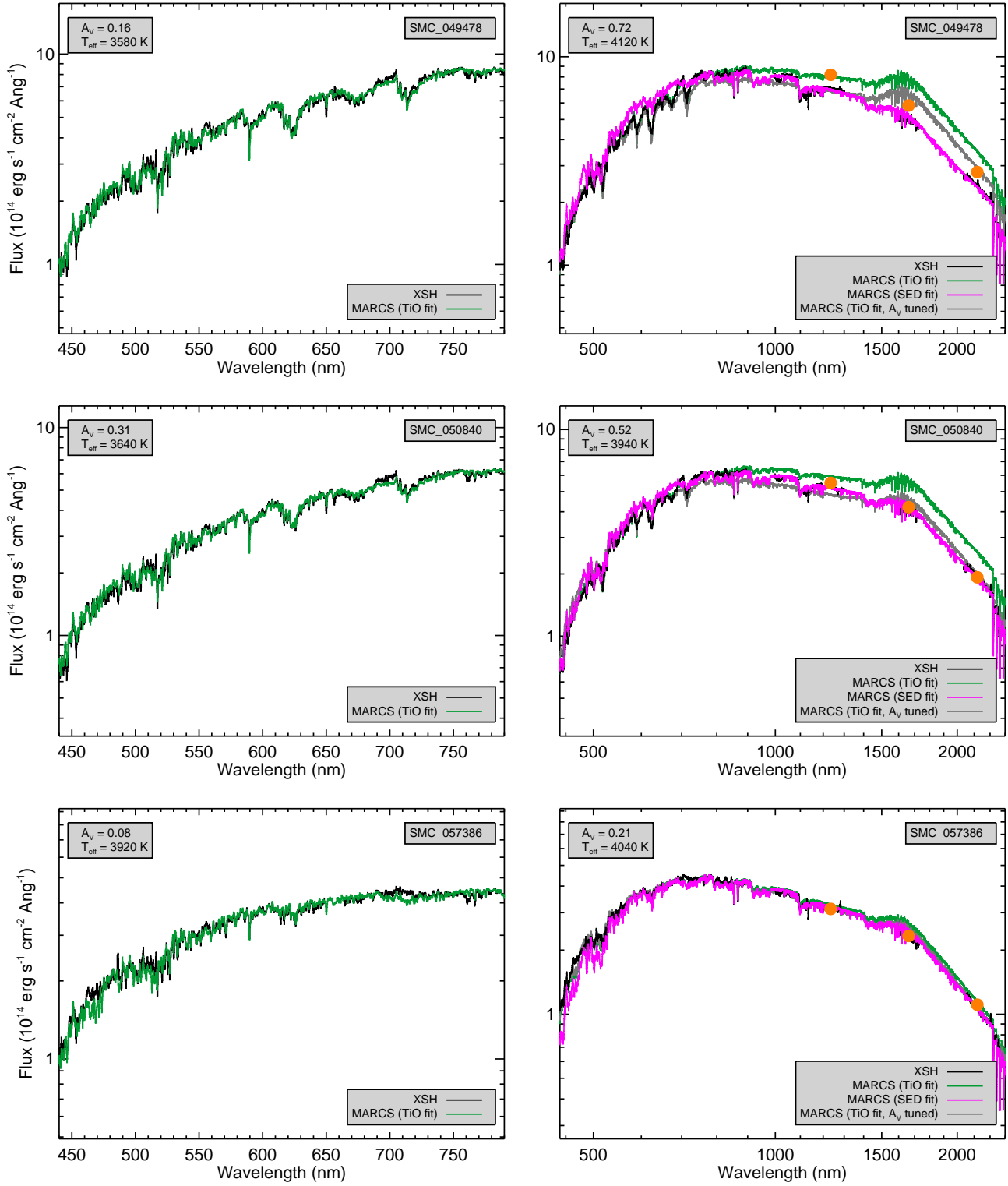


FIG. 9.— Continued.